SYNTHESIZING CATION DOPED STABLE ALPHA NICKEL HYDROXIDE HAVING LOW SELF DISCHARGE RATE BY CHEMICAL PRECIPITATION

A THESIS SUBMITTED TO
THE GRADUATE SCHOOL OF NATURAL AND APPLIED SCIENCES
OF
MIDDLE EAST TECHNICAL UNIVERSITY

BY

TURAN ILHAN

IN PARTIAL FULFILLMENT OF THE REQUIREMENTS
FOR
THE DEGREE OF MASTER OF SCIENCE
IN
METALLURGICAL AND MATERIALS ENGINEERING

FEBRUARY 2022

Approval of the thesis:

SYNTHESIZING CATION DOPED STABLE ALPHA NICKEL HYDROXIDE HAVING LOW SELF DISCHARGE RATE BY CHEMICAL PRECIPITATION

submitted by **TURAN ILHAN** in partial fulfillment of the requirements for the degree of **Master of Science** i**n Metallurgical and Materials Engineering, Middle East Technical University** by,

Prof. Dr. Halil Kalıpçılar
Dean, Graduate School of **Natural and Applied Sciences** _____

Prof. Dr. Cemil Hakan Gür
Head of the Department, **Met. And Mat. Eng., METU** _____

Assist. Prof. Dr. İshak Karakaya
Supervisor, **Met. And Mat. Eng., MET** _____

Examining Committee Members:

Prof. Dr. Kadri Aydınol
Metallurgical and Materials Eng, METU _____

Prof. Dr. İshak Karakaya
Metallurgical and Materials Eng, METU _____

Assoc. Prof. Dr. Metehan Erdoğan
Metallurgical and Materials Eng, YBU _____

Assist. Prof. Dr. Çiğdem Toparlı
Metallurgical and Materials Eng, METU _____

Assist Prof. Dr. Yusuf Keleştemur
Metallurgical and Materials Eng, METU _____

Date: 11.02.2022

I hereby declare that all information in this document has been obtained and presented in accordance with academic rules and ethical conduct. I also declare that, as required by these rules and conduct, I have fully cited and referenced all material and results that are not original to this work.

Name Last name : Turan İlhan

Signature :

ABSTRACT

SYNTHESIZING CATION DOPED STABLE ALPHA NICKEL HYDROXIDE HAVING LOW SELF DISCHARGE RATE BY CHEMICAL PRECIPITATION

Ilhan, Turan
Master of Science, Metallurgical and Materials Engineering
Supervisor : Prof. Dr. Ishak Karakaya

February 2022, 64 pages

Nickel hydroxide is one of the commonly used active material in batteries and supercapacitors. It has two phases which are α-$Ni(OH)_2$ and β-$Ni(OH)_2$. The alpha phase has higher electrochemical performances due to its higher oxidation state but it has poor stability, chargeability and self-discharge performances. Studies in both industry and academiy is focusing on to solve those problems. Effects of cation doping and starting precursor on those problems were investigated in this study. Materials were synthesized by chemical co-precipitation method which is suitable for mass production. Co, Al and Mn were used as doping agents; $Ni(NO_3)_2$, $Ni(SO_4)_2$ and NiCl were used as starting precursors. Results show that low level of Co doping was enough to obtain better electrochemical performance but higher doping level of aluminum is required. Mn was acting as β-$Ni(OH)_2$ stabilizer. Therefore, synthesizing parameters and the amount of doping level must be controlled carefully if manganese is used as dopant. In the case of starting precursors, all of them shows different eletrochemical properties but $(SO_4)^{-2}$ intercalated $Ni(OH)_2$ has poor performance than others.

Keywords: Alkaline Batteries, Nickel Based Cathode, α-$Ni(OH)_2$, Stability

ÖZ

KİMYASAL ÇÖKTÜRME YÖNTEMİ İLE DÜŞÜK SELF DEŞARJA SAHİP KATYON KATKILANMIŞ KARARLI ALFA NİKEL HİDROKSİT SENTEZİ

İlhan, Turan
Yüksek Lisans, Metalurji ve Malzeme Mühendisliği
Tez Yöneticisi: Prof. Dr. Ishak Karakaya

Şubat 2022, 64 sayfa

Nikel hidroksit, pillerde ve süper kapasitörlerde yaygın olarak kullanılan bir aktif malzemedir. Bu malzemenin iki ayrı fazı bulunmaktadır; α-$Ni(OH)_2$ ve β-$Ni(OH)_2$. Alfa fazı, yüksek yükseltgenme basamağına sahip olması nedeniyle daha iyi elektrokimyasal performansa sahiptir ancak çevrim kararlılığı, şarj edilebilirlik ve yüksek self deşarj problemlerine sahiptir. Endüstride ve akademide yürütülen çalışmalar, alfa fazına ait bu sorunları çözmek üzerine odaklanmaktadır. Bu çalışmada, katyon katkılamanın ve sentez başlangıç malzemelerinin bu problemlerin çözümüne olan etkisi incelenmiştir. Malzeme sentezi, seri üretime uygun bir yöntem olan eş çöktürme yöntemiyle yapılmıştır. Co, Al ve Mn elementleri katkılama ajanı olarak kullanılmıştır. $Ni(NO_3)_2$, $Ni(SO_4)_2$, NiCl ise başlangıç malzemesi olarak kullanılmıştır. Sonuçlar göstermektedir ki düşük katkılama seviyelerinde Co faydalıyken Al kullanılması durumunda katkılama seviyesinin artırılması gerekmektedir. Mn ise β-$Ni(OH)_2$ oluşumunu kararlı kılmaktadır. Dolayısıyla katkılama ajanı olarak Mn kullanılması durumunda katkılama seviyesine ve sentez parametrelerine özellikle önem gösterilmelidir. Başlangıç malzemelerinin her biri farklı elektrokimyasal karakteristikte davranmıştır ancak $(SO_4)^{-2}$ interkalasyonunun olduğu α-$Ni(OH)_2$, diğer malzemelere göre daha kötü bir performans sergilemiştir.

Anahtar Kelimeler: Alkali piller, nikel katot malzemesi, α-$Ni(OH)_2$, kararlılık

To my family,

ACKNOWLEDGMENTS

First, I would like to thank Prof. Dr. İshak Karakaya who help me become an engineer and who installed the discipline of being an engineer.

I would like to thank Prof. Dr. Kadri Aydınol thanks to him contribution to learn characterization of a battery and Olgun Yılmaz for the help of SEM characterizations.

This study was funded by ASPİLSAN and I would like to thank ASPİLSAN team.

I would like to thank my family because they devote themself to their children. Although they do not have any education about science, they always promote my scientific interest.

Last but not least, above all, I would like to thank Mustafa Kemal Atatürk. Thanks to him we all are individuals and not enslaved by a family or a ruler. As he said:

“Scientia Dux Vitae Certissimus”

TABLE OF CONTENTS

ABSTRACT v

ÖZ vii

ACKNOWLEDGMENTS x

TABLE OF CONTENTS xi

LIST OF TABLES xiii

LIST OF FIGURES xiv

1 INTRODUCTION 1

1.1 Energy Storage and Nickel Based Batteries 1

1.2 Aim of This Work 3

2 LITERATURE REVIEW 5

2.1 α-$Ni(OH)_2$ and β-$Ni(OH)_2$ 5

2.1.1 Self-Discharge Mechanisms 12

2.1.2 Effects of Doping on the Performance of α-$Ni(OH)_2$ 13

2.1.3 Effects of Synthesis Parameters on α-$Ni(OH)_2$ 16

3 EXPERIMENTAL PROCEDURE 19

3.1 Material Synthesis 19

3.2 Characterization 24

3.3 Electrode Preparation and Cell Assembly 26

4 RESULTS AND DISCUSSION 29

4.1 Structural Characterization 29

4.1.1 Stress Analysis 33

4.2 Effects of Doping and Precursor on Chargeability and Capacity 34

4.3 Effects of Doping and Precursor on Self-Discharge 45

4.4 Morphological Characterization and Tap Density 48
4.5 Effects of Precursor and Doping on Stability 51
5 CONCLUSION 57
REFERENCES 59

LIST OF TABLES

TABLES

Table 2-1. Crystallographic properties of α-$Ni(OH)_2$ and β-$Ni(OH)_2$. 7
Table 2-2. Activation procedure of $Ni(OH)_2$ 9
Table 2-3. Electrolytes and separators 12
Table 2-4. Synthesis parameters in literature 18
Table 3-1. Materials used in synthesis 19
Table 3-2. Synthesis parameters in study 21
Table 3-3. Target stoichiometries and nomenclature of samples 23
Table 3-4. Characterization methods 25
Table 3-5. Materials used for cell assembly 27
Table 4-1. Qualitative stress analysis from XRD 34
Table 4-2. Dicharge capacities of samples 34
Table 4-3. Peak positions $(NO_3)^{-1}$ based %30 doped samples. 36
Table 4-4. Slope of the Ia vs. sqr(Scan Rate) graph for $(NO_3)^{-1}$based samples 41
Table 4-5. Number of electrons that is involved in reaction 42
Table 4-6. Self-discharge rate of samples 46
Table 4-7. Tap density of samples 48
Table 4-8. EDS results of samples 48
Table 4-9. 2θ Diffraction angle of samples 49

LIST OF FIGURES

FIGURES

Figure 2-1. Phase changes of $Ni(OH)_2$ 5
Figure 2-2. Crystal structure of β-$Ni(OH)_2$ 6
Figure 2-3. Crystal structure of α-$Ni(OH)_2$ 6
Figure 2-4. Ionic conductivity of KOH solution for different molarities 10
Figure 2-5. Interstratified phase 15
Figure 2-6. pH range of $Ni(OH)_2$ precipitation 17
Figure 3-1. Synthesis setup 20
Figure 3-2. Setup for Mn-Dopes synthesis 20
Figure 3-3. Filtering system 22
Figure 3-4. Samples synthesized in study 24
Figure 3-5. Custom made three electrode setup 26
Figure 3-6. Slurry preperation and electrodes 27
Figure 3-7. Custom made cell 28
Figure 4-1. Diffractogram of non-dopes samples 29
Figure 4-2. Diffractogram of cobalt doped $(NO_3)^{-1}$ base samples 30
Figure 4-3. Diffractogram of aluminum doped $(SO_4)^{-2}$ based samples 30
Figure 4-4. Diffractogram of manganese doped $(NO_3)^{-1}$based samples 31
Figure 4-5. Diffractogram of aluminum doped chlorine based samples 31
Figure 4-6. Diffractogram of $(SO_4)^{-2}$ and $(SO_4)^{-2}$-30Mn 33
Figure 4-7. CV of $(NO_3)^{-1}$ based %30 doped samples. 36
Figure 4-8. CV of %10 Al doped samples. 37
Figure 4-9. CV of $(SO_4)^{-2}$-30Al. 38
Figure 4-10. EIS of Cl and Cl^{-1}-10Co 40
Figure 4-11. Ia vs. sqr(Scan Rate) for $(NO_3)^{-1}$ based samples 41
Figure 4-12. Discharge curve of $(NO_3)^{-1}$ based samples 43
Figure 4-13. EIS of $(NO_3)^{-1}$ based samples 44
Figure 4-14. Self-dischare measurement of $(NO_3)^{-1}$ 45
Figure 4-15. Ia vs. sqr(scan rate) plot of $(NO_3)^{-1}$ and Cl^{-1} 47

Figure 4-16. SEM images of samples 50
Figure 4-17. Stability curve of un-doped samples 52
Figure 4-18. Effects of Co doping on stability. 53
Figure 4-19. Effect of Co doping on the stability of $(SO_4)^{-2}$ based sample 54
Figure 4-20. Effect of Al doping on the stability of $(NO_3)^{-1}$ based sample 55
Figure 4-21. Effect of Al doping on the stability of $(SO_4)^{-2}$ based sample..... 56

CHAPTER 1

INTRODUCTION

1.1 Energy Storage and Nickel Based Batteries

The importance of energy storage technology is increasing day by day. Nowadays, companies and countries furnish more funds on renewable energy to solve the global warming problem. One of the main trouble with renewable energy is the security of supply. In other words, if there is no wind and no sun, it means there is no energy. The only solution to provide security of energy supply is to store energy. Electrochemical energy storage systems, batteries, come to the forefront for energy storage. Besides renewable energy storage, mobility is one of the main terms in daily life. Mobility is very important for civil and military applications. That is why electrochemical energy storage is vital for modern life.

There are too many options for electrochemical energy storage applications. Mainly chemistry of batteries can be summarized as follow [1]:

- Lithium ion technology; $LiNi_xMn_yCo_{(1-x-y)}O_2$ (NMC), $LiFePO_4$ (LFP), $LiNi_xCo_yAl_{(1-x-y)}O_2$ (NCA)
- Nickel based alkaline batteries; nickel metal hydride (Ni-Mh), Ni-Cd, Ni-Fe, Ni-Zn
- Lead acid
- Metal air; lithium air, ainc air, aluminum air
- Sodium ion technology
- Others; flow batteries, molten salt batteries

Lithium ion technology is the hottest topic in above list due to its higher capacity and higher discharge voltage. Upon the heels of lithium ion technology, nickel based batteries also have importance. Among the nickel based batteries, Ni-Mh is used in consumer and household electronics due to its high energy density (than other nickel based batterie) and higher safety (than lithium ion tehnology). One of the nickel based chemistry that is used today is Ni-Cd system. This system come to the forefront by its high safety, high reliability, and high power characteristic. Both Ni-Mh and Ni-Cd systems are utilizing $Ni(OH)_2$ as cathode active material and reactions of these batteries are given in Equation 1 and Equation 2 respectively, the product on the right hand side of these reactions are being formed during discharging.

$$NiOOH + MH \rightarrow M + Ni(OH)_2 \qquad \text{Equation 1}$$

$$2NiOOH + Cd + 2H_2O \rightarrow 2Ni(OH)_2 + Cd(OH)_2 \qquad \text{Equation 2}$$

There are two different phases of $Ni(OH)_2$ which are α-$Ni(OH)_2$ and β-$Ni(OH)_2$. The beta form is used in commercial applications thanks to its higher stability but studies to commercialize α-$Ni(OH)_2$ as cathode active material is continuing since it has higher capacity than beta form. Unfortunately, there are problems associated with α-$Ni(OH)_2$ which can be summarized as follow:

- Poor stability in alkaline electrolyte
- High oxygen evolution during the charge
- High self-discharge rate

Because of the above mentioned problems, α-$Ni(OH)_2$ could not be commercialized. and there are many studies that aim to solve those problems [2, 3, 4].

1.2 Aim of This Work

The main aim of this study was to investigate and solve the problems associated with α-$Ni(OH)_2$. Effects of starting precursor, doping element and level of doping on solution of aforementioned problems that associated with α-$Ni(OH)_2$ were investigated. In accordance with this purpose, different stoichiometries were synthesized with different precursors and doping agents.

Synthesizing process and doping agents were chosen from materials that are abundant and readily available such as cobalt, manganese and aluminum to develop a material that can be commercialized. The process is also vital to commercialize a material. Chemical co-precipitation, used for commercial applications, was applied to synthesize active material in this study. In addition to doping, the effects of starting precursors were also investigated because intercalated anion is one of the major parameters that affect the performance of α-$Ni(OH)_2$. Following characterization methods were applied to understand the effects of doping and precursor on the performance of active material: X-Ray Diffraction, Scanning Electron Microscopy, galvanostatic charge-discharge, electrochemical impedance spectroscopy, tap density measurement and self-discharge measurement.

CHAPTER 2

LITERATURE REVIEW

2.1 α-Ni(OH)$_2$ and β-Ni(OH)$_2$

Two phases of nickel hydroxide were characterized by Bode et.al [5] for the first time. The cycle of Ni(OH)$_2$ and phase changes during the charge and discharge is shown in Figure 2-1.

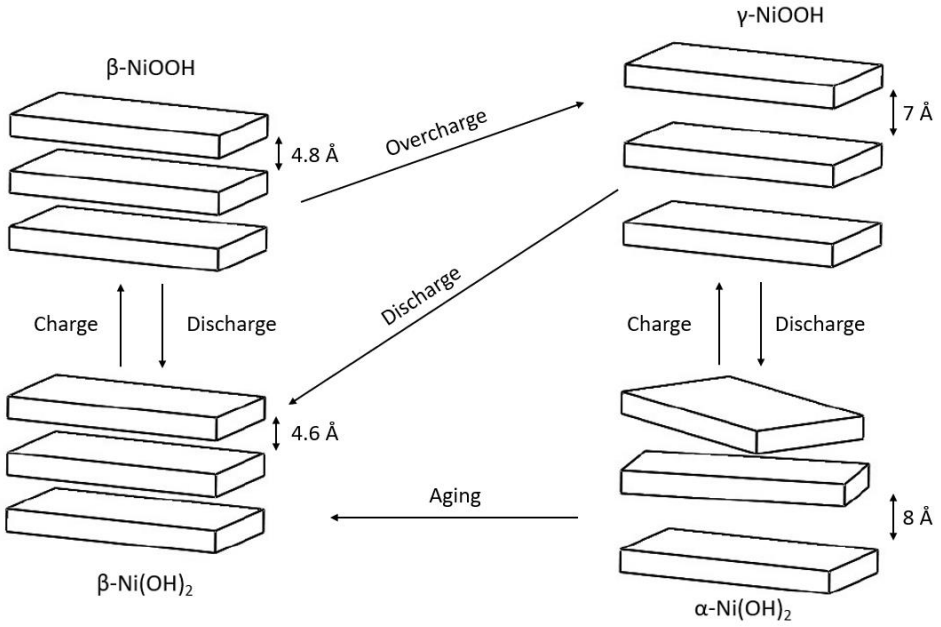


Figure 2-1. Phase changes of Ni(OH)$_2$ [6].

During charging, the β-Ni(OH)$_2$ transforms into the β-NiOOH, and the α-Ni(OH)$_2$ phase transforms into the γ-NiOOH. During discharge, the reverse of these transformations takes place. Both of these two phases have hexagonal crystal

structure and it can be seen in Figure 2-2 and Figure 2-3 respectively. Drawings were made with software VESTA.

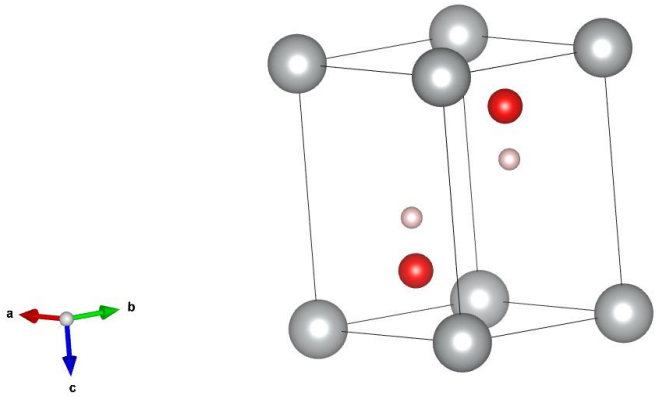


Figure 2-2. Crystal structure of β-$Ni(OH)_2$, grey (The biggest) balls are nickel, red ones (medium size) oxygen and pink spheres (the smallest) represents hydrogen [7]

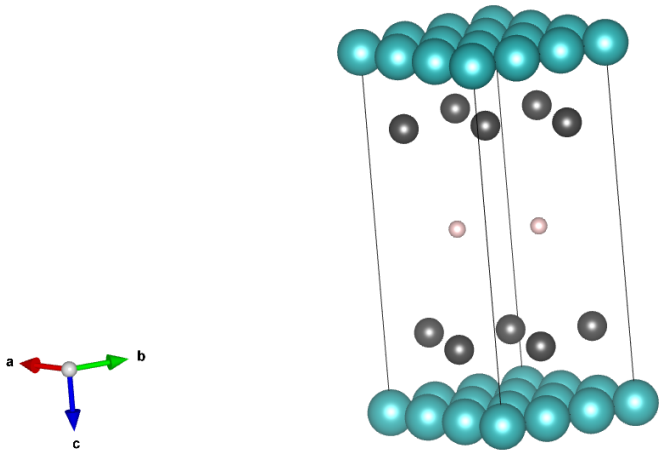


Figure 2-3. Crystal structure of α-$Ni(OH)_2$. green spheres (the biggest) show nickel atoms, black color (medium size) represents oxygen and pink spheres (the smallest) represent intercalated water or anions [7].

Since α-$Ni(OH)_2$ phase is including intercalated water or anion, it has a higher c-parameter than that of β-$Ni(OH)_2$. Hall et al. [7] summarized the crystallographic properties of α-$Ni(OH)_2$ and β-$Ni(OH)_2$, and the results are given in Table 2-1.

Table 2-1. Crystallographic properties of α-$Ni(OH)_2$ and β-$Ni(OH)_2$ [7].

	β-$Ni(OH)_2$	α-$Ni(OH)_2$
Space Group	No.164	No.162
a=b	3.12Å	3.08Å
c	4.61Å	8.00Å

According to the studies, the intercalated anions significantly change the c-parameter of nickel hydroxide. It is found that if only nitrate is intercalated in Ni-Mh double layer hydroxide (if nickel hydroxide is doped with any metal, it is called double layer hydroxide) interlayer spacing $d_{average}$=7.38Å while it can be increased up to 28.41Å by intercalating more than one anion. It is reported that as the distance between the layers increases, the capacity of the material also increases [8].

Although α-$Ni(OH)_2$ and β-$Ni(OH)_2$ have the same crystal structure, the alpha phase has a higher discharge capacity. The main reason behind that phenomenon is that charged alpha phase (γ-NiOOH) has a higher oxidation state than that of the fully charged beta phase (β-NiOOH). During the charging of the beta phase, Ni^{+2} is oxidized to Ni^{+3} while nickel in α-$Ni(OH)_2$ is oxidizing from Ni^{+2} to Ni^{+4}. The theoretical capacity of the first reaction is 289 mAh/g and the second case has a much higher theoretical capacity. Although the oxidation state of the alpha phase is +4, 2 electrons do not react in practical applications. As an example, in a study oxidation state of Ni in γ-NiOOH is found as +3.5 and it means that practical capacity is lower than the theoretical value [9]. In another study, oxidation state was found as +3.67 and it yields 483 mAh/g capacity, and this capacity is one of the highest capacity which is obtained in the literature [10]. The oxidation state and capacities of the materials considerably change due to synthesizing parameters and different crystallographic properties.

Although α-$Ni(OH)_2$ has promising performance, there is no known commercial application of it. The main problems with the alpha phase are low stability in alkaline environment (rapid capacity degradation during cycling), poor self-discharge, poor

chargeability, and poor tap density. Since the alpha phase has higher c-parameter than the beta phase, it has lower packing density, that is why it has lower tap density than the beta phase.

α-$Ni(OH)_2$ loses its intercalated water and anions in dehydrative media, such as alkaline electrolytes. Therefore it turns into the beta phase, this is the main explanation of poor stability [11].

An activation procedure must be applied to both α-$Ni(OH)_2$ and β-$Ni(OH)_2$ to utilize material properly. Although the advantage of the activation process is clear, the mechanism of that process is not clearly understood. Most studies in that field are done empirically. According to a study, the activation process increases proton diffusion coefficient and decreases charge transfer resistance. It is claimed that if the activation process is applied in a galvanostatic way with a low current rate, the structure becomes more porous and ion channels become more open [12]. A study which is focusing on the time required for the activation process shows that as the molarity of electrolyte increases, the material becomes active more rapidly. This is explained by the diffusion controlled nature of the activation process [13]. It is found that if the activation process is done properly, the internal resistance of the cell decreases due to increasing conductivity. This phenomenon is readily observed in cobalt doped $Ni(OH)_2$. The surface of the electrode is coated with a conductive CoOOH layer during the activation process [14, 15].

Although both α-$Ni(OH)_2$ and β-$Ni(OH)_2$ require an activation process, it takes longer time in α-$Ni(OH)_2$. It is explained by the sluggish anion exchange mechanism which is valid for the alpha phase. In the beta phase (in the case of there is no intercalated anion), OH^- ions are reacting with H^+ which is released from $Ni(OH)_2$, and water is formed. But if there is any anion intercalation, anion exchange is required before the reaction of H^+ and OH^- and it slows down the reaction rate. If the intercalated anion has higher anion exchange ability, such as Cl^{-1}, the activation process becomes more rapid [16]. Activation of $Ni(OH)_2$ is done as galvanostatic

charge-discharge. Some of the applied procedure which is found in the literature is summarized in Table 2-2.

Table 2-2. Activation procedure of $Ni(OH)_2$

	Charge Current/Cut-off Condition	Discharge Current/Cut-off Condition	Reference Electrode	Cycle	Reference
1	0.5C/No Data	0.5C/0.2V	Hg/HgO	Until capacity is stabilized	[17]
2	0.1C/No Data	0.1C/1V	Hydrogen storage alloy	5	[16]
3	0.2C/%120 SOC	0.2C/1V	Hydrogen storage alloy	20	[18]
4	0.2C/No Data	0.2C/1V	Hydrogen storage alloy	15	[19]
5	0.2C/%120 SOC	0.2C/1V	Hydrogen storage alloy	15	[16]

In nickel based batteries, alkaline solution (usually KOH-Water or NaOH-Water) is used as electrolyte. Since it has higher ionic conductivity, KOH is used as electrolyte salt mainly. For battery applications, the main criteria to select electrolyte is its ionic conductivity. It is shown that the best ionic conductivity for KOH-Water solution at room temperature is obtained at 6M as it is shown in Figure 2-4. [19]

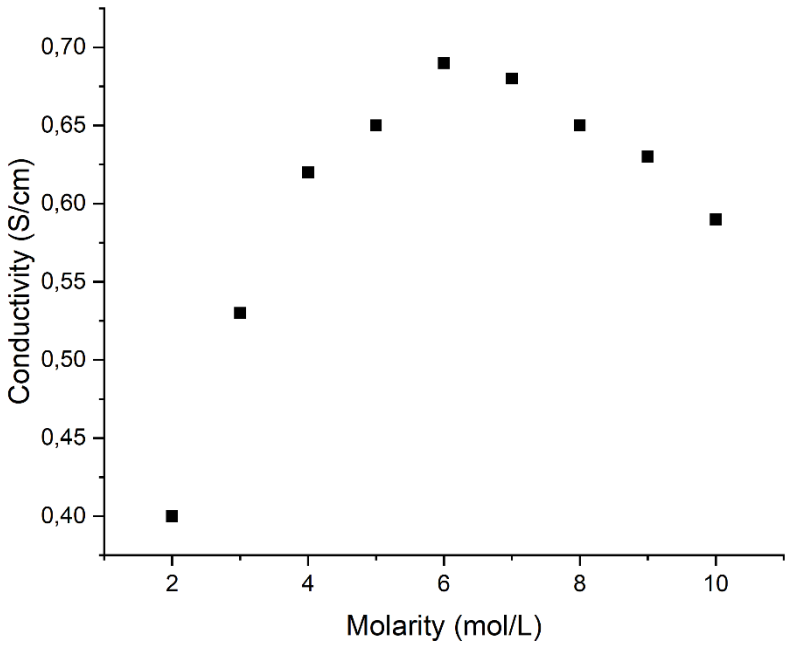


Figure 2-4. Ionic conductivity of KOH solution for different molarities [19]

In Ni-Mh and Ni-Cd batteries, the end-of-charge voltage can rise to 1.6V. Electrolysis-induced electrolyte degradation is an important problem in these batteries using water-based electrolytes. The electrolysis reaction is shown in Equation 3.

$$4OH^- \rightarrow O_2 + 2H_2O + 4e^- \qquad \text{Equation 3}$$

Equation 3 caused premature degradation of electrolyte and poor charge acceptance of cathode material. Some portion of the applied current is consumed by oxygen evolution reaction which is shown in Equation 4.

$$I_{OER} = I^0_{OER} \times X \exp\left(\alpha_{OER} \frac{nF}{RT}(E_{OX} - E_{OER})\right) \qquad \text{Equation 4}$$

I_{OER}, the current which is used for oxygen evolution reaction (OER); I^0_{OER}, exchange current density; α, transfer coefficient; E_{OX} oxidation potential of $Ni(OH)_2$; E^0_{OER},

oxygen evolution potential. The difference between cathode oxidation potential and oxygen evolution potential and (E_{OX}-E_{OER}) must be low (more negative) to decrease side reaction current (I_{OER}) and to increase charge acceptancy of cathode. In other words, oxygen evolution potential must be more positive to obtain better chargeability [20].

There are varying strategies to repress oxygen evolution in nickel based batteries. These strategies can be summarized as follow:

- Electrolyte additives
- Doping cathode with other metals
- Intercalating different anions

The precursor that is used for material synthesizing determines which anion will be intercalated into α-$Ni(OH)_2$. It is shown that some of the anions increase oxygen evolution potential and make (E_{OER}-E_{OX}) more positive. Effects of different anions on the oxygen evolution rate are as follows:

$(CO_3)^{-2}$, $(SO_4)^{-2}$, $(OH)^{-1}$, $(NO_3)^{-1}$, $(Cl)^{-1}$ [lowest OER is in Cl^{-1}, [16]

One of the problems associated with oxygen evolution is the recombination reaction in nickel batteries. The oxygen which is released from the cathode goes to the anode side and oxidizes the anode material. This phenomenon is observed in both Ni-Mh and Ni-Cd, Equation 5 shows recombination reaction in Ni-Cd systems.

$$3Cd + O_2 + 2OH^- + 2H_20 \rightarrow 3Cd(OH)_2 + 2e^- \qquad \text{Equation 5}$$

Oxidation of anode due to recombination reaction is a type of discharge reaction. As a result of recombination, cell voltage begins to drop and this is called “Negative deltaV”. This is used as a charging cut-off condition in nickel based batteries. One of the commercially and academically applied strategies to repress oxygen evolution reaction is using Li(OH) as an additive for the electrolyte. It is proved that Li(OH) addition increases the oxygen evolution potential, thereby the chargeability of the

cathode increases [21]. Some of the electrolyte composition which is commonly used is summarized in Table 2-3.

Table 2-3. Electrolytes and separators

	Molarity and Additive	Separator	Reference
1	6M KOH+15g/L LiOH	PP	[16]
2	6M KOH+1M LiOH	Polyolefine	[17]
3	6M KOH+0.5M LiOH	PP	[18]
4	6M KOH+0.6M LiOH	PP	[19]
5	30%KOH+1%LiOH (wt%)	PP/PE	[20]

2.1.1 Self-Discharge Mechanisms

Ikoma et al. summarized self-discharge mechanisms of nickel based batteries as follow [22]

- Decomposition of NiOOH to $Ni(OH)_2$
- Shuttle reactions
- Impurities (that causes redox reaction in the cell)
- Dissolution of metal

Studies show that the first two of the above reactions are more dominant than others. Organic impurities are usually caused by separator and residual impurities from synthesizing process. The separator material must be chosen carefully to hinder self-discharge caused by the separator. It is known that some of the separators do not have chemical stability in alkaline environment, and these separators cause the formation of amine and ammonia groups that causes shuttle reactions in the cell. PP is considered one of the most suitable separators for nickel batteries. The shuttle reactions which are given below were characterized by Shukla. [23]

$$NO_3^- + H_2O + 2e^- \rightarrow NO_2^- + 2OH^- \qquad \text{Equation 6}$$

$$NO_2^- + 5H_2O + 6e^- \rightarrow NH_3 + 7OH^- \qquad \text{Equation 7}$$

$$NO_3^- + 3Cd + 5H_2O \rightarrow NH_3 + 3Cd(OH)_2 + OH^- \quad \text{Equation 8}$$

$$NH_3 + 7OH^- \rightarrow NO_2^- + 5H_2O + 6e^- \quad \text{Equation 9}$$

$$NH_3 + 6NiOOH + H_2O + OH^- \rightarrow NO_2^- + 6Ni(OH)_2 \quad \text{Equation 10}$$

$$NO_2^- + 2NiOOH + H_2O + \rightarrow NO_2^- + 2Ni(OH)_2 + NO_3^- \quad \text{Equation 11}$$

The above reactions are known as shuttle reactions. The $Ni(OH)_2$ powder must be washed properly (to get rid of impurities such as nitrate and nitrite) to decrease the rate of self-discharge caused by shuttle reactions. Equation 12 shows the primary reason for self-discharge in nickel batteries, which is the decomposition of NiOOH to $Ni(OH)_2$.

$$NiOOH + \frac{1}{2}H_2O \rightarrow Ni(OH)_2 + \frac{1}{4}O_2 \quad \text{Equation 12}$$

According to Bernard and Lipperd, the equilibrium potential of $NiOOH/Ni(OH)_2$ (at ph.14) is 0.49V (vs Standart Hydrogen Electrode) and oxygen evolution potential is 0.40 at the same conditions [24]. It means that, in a fully charged nickel battery, cell potential is enough for oxygen evolution. To hinder self-discharge caused by oxygen evolution, E_{OER} must be increased or E_{OX} must be decreased. Increasing E_{OER} is a better way since a decrease in E_{OX} also causes a decrease in cell voltage thereby energy density of the battery becomes poorer. Additionally, oxygen evolution from the cathode also causes self-discharge of the anode according to Equation 5. In summary, oxygen evolution in nickel based batteries must be hindered to obtain better chargeability and self-discharge performance.

2.1.2 Effects of Doping on the Performance of α-$Ni(OH)_2$

The major strategy to solve Alpha phases' intrinsic problems (poor stability, and high self-discharge) is to dope it with cations. Aluminum and cobalt are used mainly as doping agents. The effectiveness of cobalt is well known but it is desired to be replaced by aluminum due to low cost and environmental concerns.

Cobalt is still used widely in the battery industry although it is toxic and expensive. The main advantages and function of cobalt as a doping agent in α-$Ni(OH)_2$ can be summarized as follow:

1. During the activation cycle, it is oxidized and the surface of the electrode is coated with CoOOH which is a highly conductive material and it decreases the impedance of the cell [24]. A higher valance state of Co helps to bind intercalated anion more strongly and increases the stability of α-$Ni(OH)_2$. Unless the cell is overdischarged, CoOOH is not reduced. It means that the advantage of Co^{+3} can be maintained for long cycles.
2. Cobalt doping makes electrode potential more negative. Oxidation of cathode begins at a lower potential. This yields higher charge acceptance and lowers oxygen evolution in charging. But one should be careful about the amount of cobalt doping since as the amount of cobalt increases, the voltage of the cell decreases. This causes lower discharge potential and lowers energy density.
3. Since it increases coulombic efficiency, it protects electrolytes from premature degradation.
4. It increases the proton diffusion coefficient by creating vacancy sites for hydrogen diffusion [24]

Alongside cobalt, aluminum is the other most popular dopant for α-$Ni(OH)_2$. Academic research mainly focuses on Al. Since it has +3 oxidation state, it is one of the best options for doping to obtain stable α-$Ni(OH)_2$. The stability mechanism of Al is the same as cobalt; a higher valance state causes excess positive charge on α-$Ni(OH)_2$ and more anions are intercalated to obtain charge neutrality. Although aluminum is effective to obtain stability, it is problematic for oxygen evolution. It increases the E_{OX}, and the difference between oxygen evolution potential and cathode oxidation potential decreases (E_{OER}-E_{OX}). Another problem associated with aluminum is poor tap density. Since it has a lower atomic weight, it decreases volumetric energy density but it must be noted that usage of such light metals increases gravimetric energy density [18]. Besides the molecular weight, the tap density of a powder depends on many other parameters.

In commercial applications, cadmium is commonly used as a doping agent for $Ni(OH)_2$, although it is highly toxic. It hinders the intercalation of water and anion during the synthesizing and charge/discharge routine. So it acts as a beta stabilizer. During the charging, $\beta \rightarrow \alpha$ transformation causes high volume change thereby particle cracking and capacity losses. Additionally, the usage of cadmium increases the conductivity of $Ni(OH)_2$ [25].

Manganese is another popular doping agent. It gives more stability to α-$Ni(OH)_2$ with the same mechanism as in the case of cobalt and aluminum. Additionally, it hinders oxygen evolution very effectively. The main shortage with the Mn is it's tendency to get oxidized during the synthesizing. To protect manganese from oxidation, synthesizing process must be done under a protective atmosphere. If it is oxidized, it causes a reduction in nickel and acts as the beta stabilizer. In such cases, some amount of β-$Ni(OH)_2$ can be formed in between α-$Ni(OH)_2$ layer. This structure is called the interstratified phase which is shown in Figure 2-5. Unlike cobalt, manganese does not change the oxygen evolution potential (in the case of cobalt both E_{OX} and E_{OER} decreases but (E_{OER}-E_{OX}) increases) this yields higher discharge potential in Mn doped α-$Ni(OH)_2$ than Co doped α-$Ni(OH)_2$. [26]

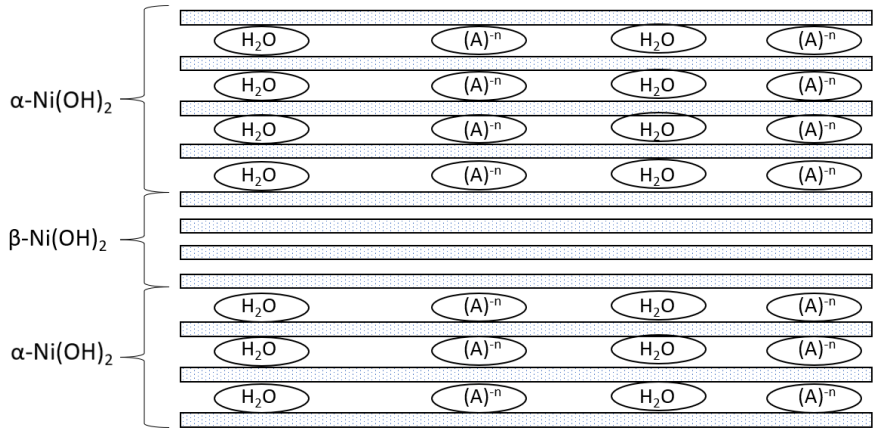


Figure 2-5. Interstratified phase. $(A)^{-n}$ denotes intercalated anion [7].

Besides the higher oxidation state of transition metals, some doping atoms may reside in tetrahedral sites and give the lattice an excess positive charge. In such a

case the formula of the $Ni(OH)_2$ can be expressed as $[Ni_{(1-x)}M_{2x}(OH)]^{2x+}$. In such a structure, the doping agent increases the stability although it has a low oxidation state. [27] It must be noted that usage of dopant decreases the amount of active mass ($Ni(OH)_2$) in total mass. That is why the amount of dopant must be controlled carefully.

2.1.3 Effects of Synthesis Parameters on α-$Ni(OH)_2$

α-$Ni(OH)_2$ can be synthesized from precursors by electrochemical and chemical co-precipitation. Since co-precipitation is more suitable for commercial applications, It is preferred as the most common synthesis method [28]. In this method, metal salts (dopant and nickel salt) are solved in water to obtain proper molarity and desired stoichiometry (amount of dopant is controlled by the amount of salts that are added to the solution). After the mother solution is ready, the pH of the solution is increased suddenly or dropwise by adding NaOH or KOH. When the pH has reached enough value to trigger the precipitation reaction, the material begins to precipitate. Some scientists prefer to use a chelating agent to chelate metals before increasing the pH of the mother solution. Since this study does not aim to optimize synthesizing, the parameter for material synthesize was taken from literature and the most common parameters were used. The major parameters for material synthesizing (in co-precipitation) can be classified as:

- pH
- Time
- Speed of stirring
- Temperature

The pH must be high enough to obtain hydroxide precipitates. In a study, it was found that the minimum pH value to get $Ni(OH)_2$ precipitation is 8, as can be seen in Figure 2-6 [29].

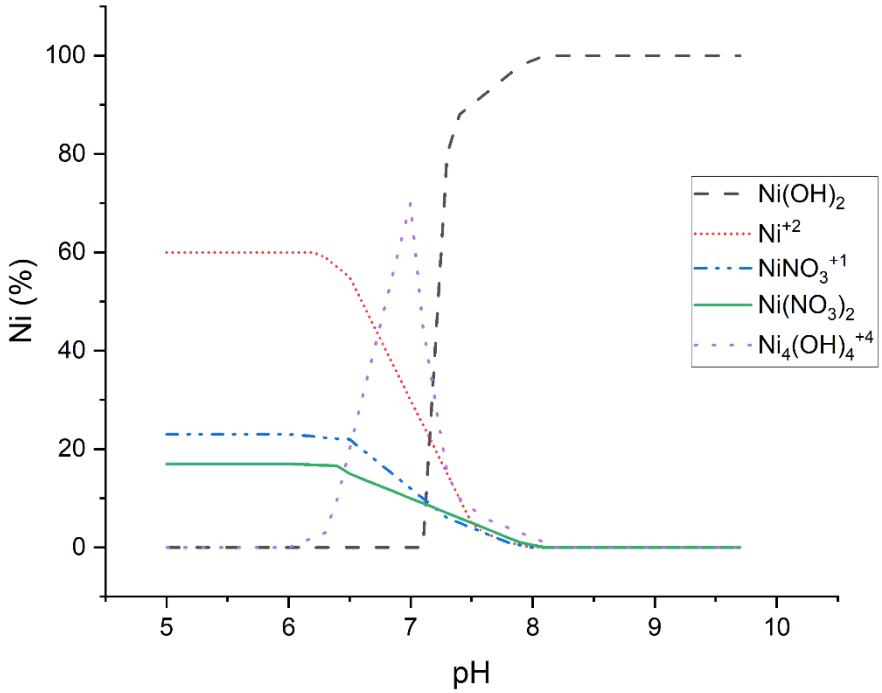


Figure 2-6. pH range of $Ni(OH)_2$ precipitation [29]

pH value does not affect the stoichiometry of the final product but it determines the particle size. As the pH value increases, particle size increases. There must be an upper limit of pH value because if the pH is too high, the product ($Ni(OH)_2$) may begin to dissolve. Additionally, α-$Ni(OH)_2$ is not stable in alkaline environment. Thus, if the pH is increased too much α-$Ni(OH)_2$ may transform into β-$Ni(OH)_2$ [29].

It is known that higher temperature makes the formation of β-$Ni(OH)_2$ more favorable. Because of that reason, α-$Ni(OH)_2$ is synthesized at low temperature, usually at room temperature. Stacking fault and interstratified phase formation begin at temperatures higher than 60 °C [7].

The last parameters that should be considered in co-precipitation are reaction time and speed of stirring. It is well known that if the reaction time is increased particle

size increases. Stirring speed determines the shape of particles. Unfortunately, there are very few studies that focus on the effects of stirring and reaction time on the performance of α-$Ni(OH)_2$. Synthesis parameters that are commonly used in the literature are summarized in Table 2-4.

Table 2-4. Synthesis parameters in the literature

	Dopant	pH Agent	Dropping Speed	pH	Temperature	Reference
1	Mn	2M NaOH	Suddenly	10-13	-	[30]
2	Al	1M NaOH	3ml/min	9-11	35 °C	[31]
3	Al, Co	NaOH	Dropwise	9	50 °C	[32]
4	Co, Zn	4M NaOH	Dropwise	-	50 °C	[33]
5	Al	NH_4OH	Dropwise	12	90 °C	[34]

CHAPTER 3

EXPERIMENTAL PROCEDURE

3.1 Material Synthesis

All the chemicals that were used for material synthesis are given in Table 3-1

Table 3-1. Materials used in the synthesis

Material	Product Code	Purpose
$Ni(NO_3)_2.6H_2O$	Alfa Aesar ACRO223155000	Precursor, Ni Source
$Ni(SO_4).7H_2O$	Sigma Aldrich 72285	Precursor, Ni Source
$NiCl.6H_2O$	Sigma Aldrich 654507	Precursor, Ni Source
$Co(NO_3)_2.6H_2O$	Sigma Aldrich 230375	Dopant, Co Source
$Al(NO_3)_3.9H_2O$	Sigma Aldrich 237973	Dopant, Al Source
$Mn(NO_3)_2.4H_2O$	Alfa Aesar A18521	Dopant, Mn Source
NaOH	Sigma Aldrich 06203	Precipitating Agent
NH_4OH	Senlab SL005432	Chelating Agent

All materials were used without purification or any other process. Material synthesis was done by chemical co-precipitation. Initially metal salts were mixed in accordance with desired stoichiometry in this method. Ammonia solution was added by peristaltic pump to the metal solution until pH reaches 7. Ammonia act as a chelating agent. Mother solution (metals and ammonia) was mixed for 30 minutes to complete chelating and NaOH solution was added to increase pH to 11.5 by a peristaltic pump. the pH of the solution was held at 11.5 for 1 hour. A picture showing the co-precipitation setup is given in Figure 3-1. The solution was mixed by a magnetic stirrer all the time during the process.

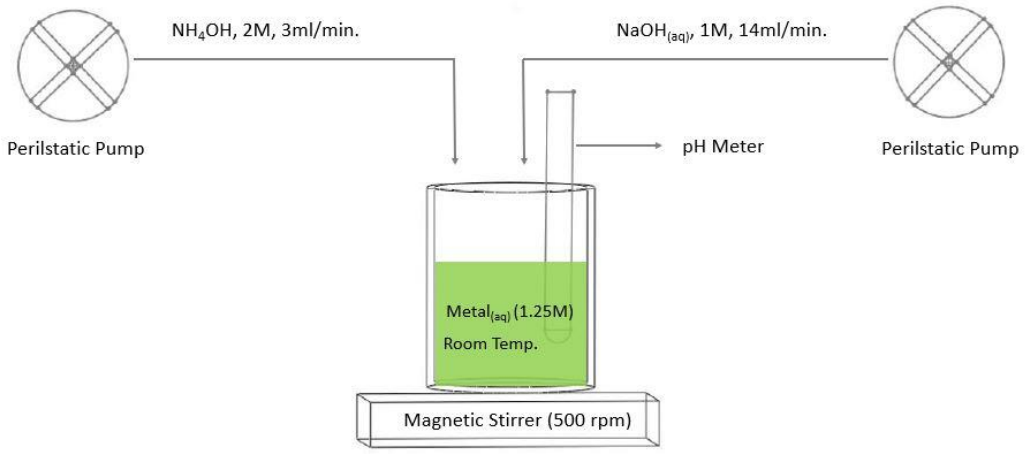


Figure 3-1. Synthesis setup

The samples which are manganese was used as a doping agent, material synthesis was done under a protective atmosphere to prevent oxidation of manganese. The picture of the setup used to prepare manganese containing samples is shown in Figure 3-2.

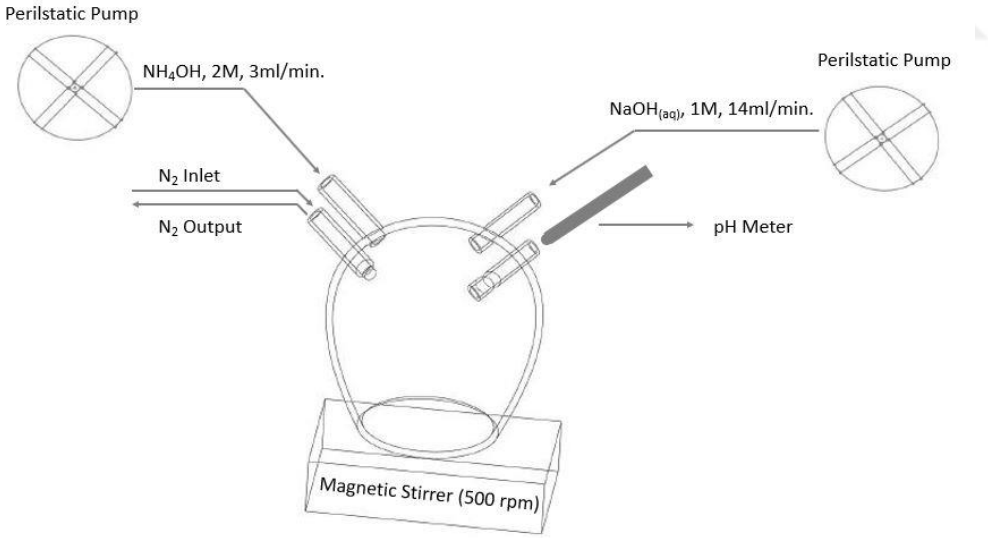


Figure 3-2. The drawing of the setup used for Mn-Doped synthesis

Other than the protective atmosphere, all the synthesis parameters were the same for all samples, including those containing manganese. Synthesis parameters are given in Table 3-2.

Table 3-2. Synthesis parameters in the co-precipitation study

Parameter	**Value**
Total Metal Molarity	1.25M
Ammonia Solution Molarity	2M
Ammonia Solution Feed Rate	3ml/minute
NaOH Solution Molarity	1M
NaOH Solution Feed Rate	14ml/minute
Holding Mother Solution at pH 7	30 minute
Holding Mother Solution at pH 11.5	60 minute
Mother Solution Stirring	500 rpm
Reaction Temperature	Room Temperature (18°C - 25°C)
Nitrogen Gas Feed Rate (Mn containing samples)	3lt/minute

After co-precipitation reaction was completed (total time 90 minutes) mother solution was filtered and washed twice with distilled water and once with ethanol as shown in Figure 3-3.

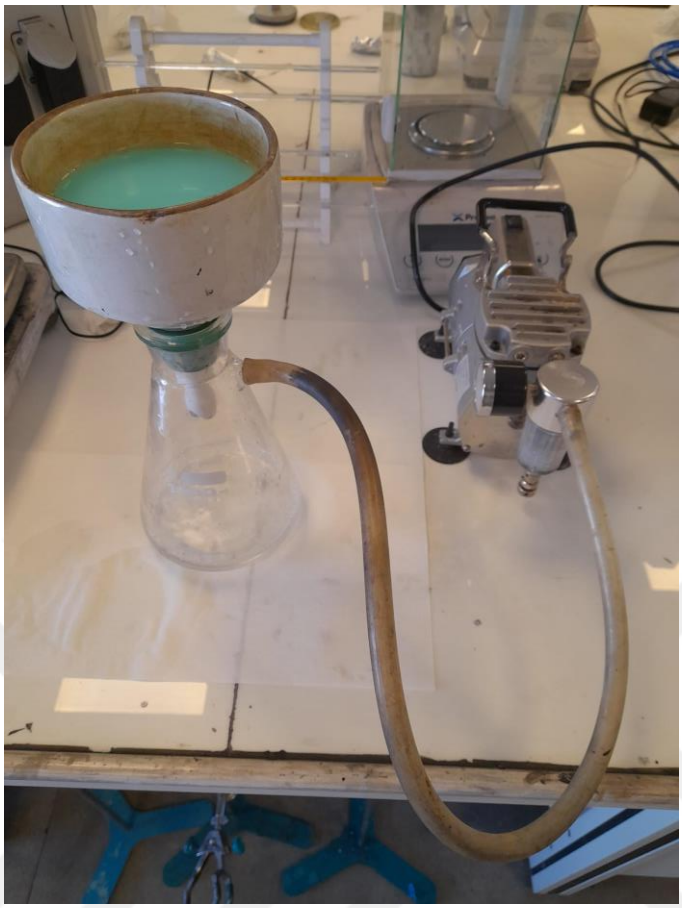


Figure 3-3. Filtering system

After filtering was done, samples were dried in air for 1 night. Precursors, doping agents, target stoichiometry, and nomenclature of samples that were synthesized can be seen in Table 3-3, Figure 3-4 shows some of those samples.

Table 3-3. Target stoichiometries and nomenclature of samples

Stoichiometry	Precursor (Ni Source)	Dopant	Nomenclature
$Ni(OH)_2$	$Ni(NO_3)_2.6H_2O$	-	$(NO_3)^{-1}$
$Ni(OH)_2$	$Ni(SO_4).7H_2O$	-	$(SO_4)^{-2}$
$Ni(OH)_2$	$NiCl.6H_2O$	-	Cl^{-1}
$Ni_{0.9}Co_{0.1}(OH)_2$	$Ni(NO_3)_2.6H_2O$	Co	$(NO_3)^{-1}$-10Co
$Ni_{0.8}Co_{0.2}(OH)_2$	$Ni(NO_3)_2.6H_2O$	Co	$(NO_3)^{-1}$-20Co
$Ni_{0.7}Co_{0.3}(OH)_2$	$Ni(NO_3)_2.6H_2O$	Co	$(NO_3)^{-1}$-30Co
$Ni_{0.9}Al_{0.1}(OH)_2$	$Ni(NO_3)_2.6H_2O$	Al	$(NO_3)^{-1}$-10Al
$Ni_{0.8}Al_{0.2}(OH)_2$	$Ni(NO_3)_2.6H_2O$	Al	$(NO_3)^{-1}$-20Al
$Ni_{0.7}Al_{0.3}(OH)_2$	$Ni(NO_3)_2.6H_2O$	Al	$(NO_3)^{-1}$-30Al
$Ni_{0.9}Mn_{0.1}(OH)_2$	$Ni(NO_3)_2.6H_2O$	Mn	$(NO_3)^{-1}$-10Mn
$Ni_{0.8}Mn_{0.2}(OH)_2$	$Ni(NO_3)_2.6H_2O$	Mn	$(NO_3)^{-1}$-20Mn
$Ni_{0.7}Mn_{0.3}(OH)_2$	$Ni(NO_3)_2.6H_2O$	Mn	$(NO_3)^{-1}$-30Mn
$Ni_{0.9}Co_{0.1}(OH)_2$	$Ni(SO_4).7H_2O$	Co	$(SO_4)^{-2}$-10Co
$Ni_{0.8}Co_{0.2}(OH)_2$	$Ni(SO_4).7H_2O$	Co	$(SO_4)^{-2}$-20Co
$Ni_{0.7}Co_{0.3}(OH)_2$	$Ni(SO_4).7H_2O$	Co	$(SO_4)^{-2}$-30Co
$Ni_{0.9}Al_{0.1}(OH)_2$	$Ni(SO_4).7H_2O$	Al	$(SO_4)^{-2}$-10Al
$Ni_{0.8}Al_{0.2}(OH)_2$	$Ni(SO_4).7H_2O$	Al	$(SO_4)^{-2}$-20Al
$Ni_{0.7}Al_{0.3}(OH)_2$	$Ni(SO_4).7H_2O$	Al	$(SO_4)^{-2}$-30Al
$Ni_{0.9}Mn_{0.1}(OH)_2$	$Ni(SO_4).7H_2O$	Mn	$(SO_4)^{-2}$-10Mn
$Ni_{0.8}Mn_{0.2}(OH)_2$	$Ni(SO_4).7H_2O$	Mn	$(SO_4)^{-2}$-20Mn
$Ni_{0.7}Mn_{0.3}(OH)_2$	$Ni(SO_4).7H_2O$	Mn	$(SO_4)^{-2}$-30Mn
$Ni_{0.9}Co_{0.1}(OH)_2$	$NiCl.6H_2O$	Co	Cl^{-1}-10Co
$Ni_{0.8}Co_{0.2}(OH)_2$	$NiCl.6H_2O$	Co	Cl^{-1}-20Co
$Ni_{0.7}Co_{0.3}(OH)_2$	$NiCl.6H_2O$	Co	Cl^{-1}-30Co
$Ni_{0.9}Al_{0.1}(OH)_2$	$NiCl.6H_2O$	Al	Cl^{-1}-10Al
$Ni_{0.8}Al_{0.2}(OH)_2$	$NiCl.6H_2O$	Al	Cl^{-1}-20Al
$Ni_{0.7}Al_{0.3}(OH)_2$	$NiCl.6H_2O$	Al	Cl^{-1}-30Al
$Ni_{0.9}Mn_{0.1}(OH)_2$	$NiCl.6H_2O$	Mn	Cl^{-1}-10Mn
$Ni_{0.8}Mn_{0.2}(OH)_2$	$NiCl.6H_2O$	Mn	Cl^{-1}-20Mn
$Ni_{0.7}Mn_{0.3}(OH)_2$	$NiCl.6H_2O$	Mn	Cl^{-1}-30Mn

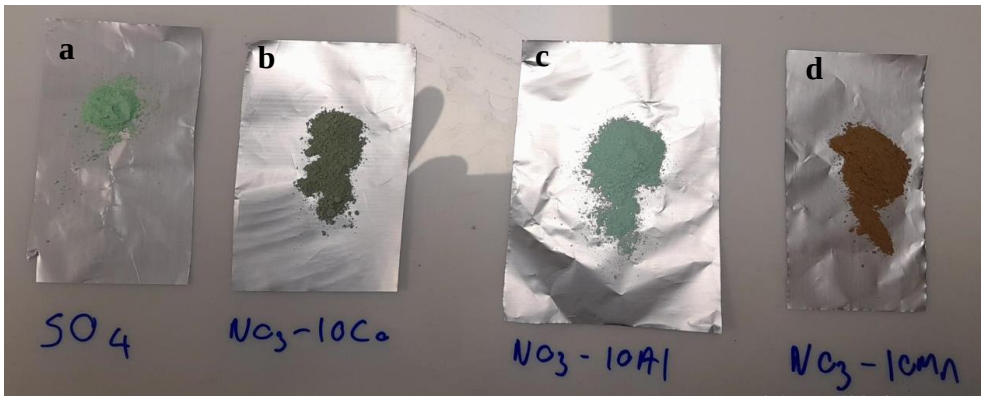


Figure 3-4. Samples synthesized in the study. a) $(SO_4)^{-2}$ sample without doping b) $(NO_3)^{-1}$ based sample with 10% Co doping c) $(NO_3)^{-1}$ based sample with 10% Al doping d) $(NO_3)^{-1}$ based sample with 10% Mn doping.

3.2 Characterization

Table 3-4 shows characterization methods and instruments that were used. Figure 3-5 shows the custom-made three-electrode setup with graphite working; platinum counter and Ag/AgCl reference electrode.

Table 3-4. Characterization methods and instruments.

Method	**Instrument**	**Detail**
Charge-Discharge	Neware BTS4000 5V50mA	Activation Current: 100mA/g (3 cycles) Charge/Discharge Current: 400mA/g Charge Cut-Off Condition: 120% of 400mAh/g Discharge Cut-off Condition: Cell Voltage=1V
Cyclic Voltammetry	Gamry Reference 3000	Reference Electrode: Ag/AgCl Scan rate: 0.25 mV/s, 0.5 mV/s, 1 mV/s, 2 mV/s
Electrochemical Impedance Spectroscopy (EIS)	Gamry Reference 3000	Initial Frequency: 30 kHz Final Frequency: 100 mHz AC Voltage RMS: 2mV
XRD	Bruker D2 Phaser	2θ: 5° - 90° Increment: 0.02° (resolution) Time/Step: 0.5s (data acquisition time/point)
Tap Density	Dahometer 100A	Amplitude: 10mm Number of Taps: 1000
SEM/EDS		Parameters depend on sample and condition

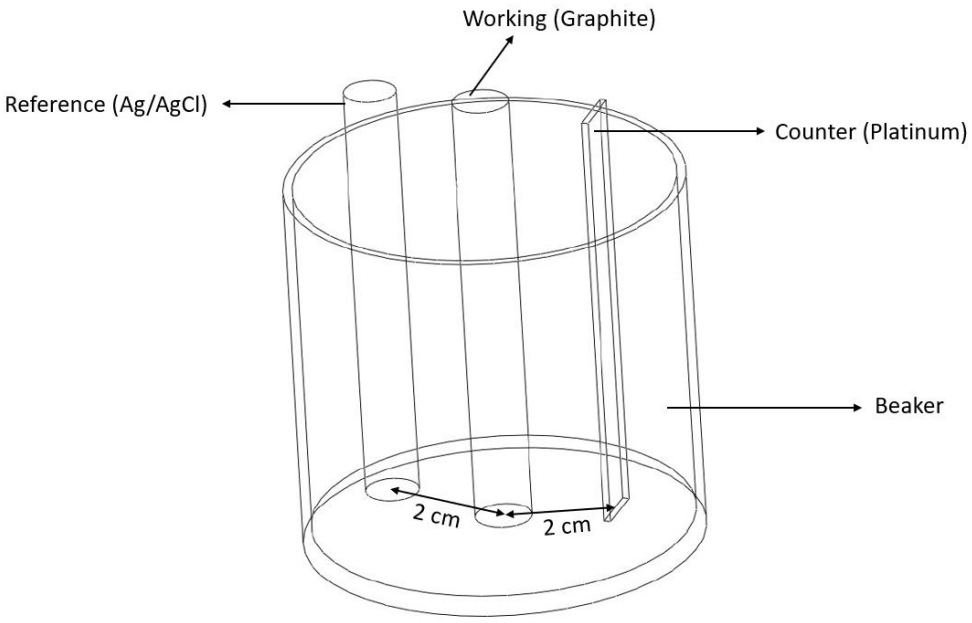


Figure 3-5. Custom made three-electrode setup

3.3 Electrode Preparation and Cell Assembly

After material synthesizing was completed, $Ni(OH)_2$ was mixed with carbon black (conductive carbon), Polyvinylidene fluoride (PVDF, binding agent) with the mass ratio 7:2:1 respectively and proper amount of n-methyl pyrrolidone (NMP) was used as the solvent. After the mixing operation was completed, the slurry was pasted on nickel foam and it was dried in an oven (115 °C and 3 hours). After the drying process, the electrodes were ready to be tested. Ball mill with stainless steel case and ball was used for mixing operation to obtain slurry as shown in Figure 3-6. Table 3-5 shows the materials that were used for cell assembly.

Table 3-5. Materials used for cell assembly

Material	Manufacturer/Product Code
Nickel Foam (thickness 1.7mm)	Anzhen Guangyi Electronic Technology
Anode	Hawker GmbH Sintered Cadmium
Separator	Hawker GmbH PP
KOH	ISOLAB 960.83.1000

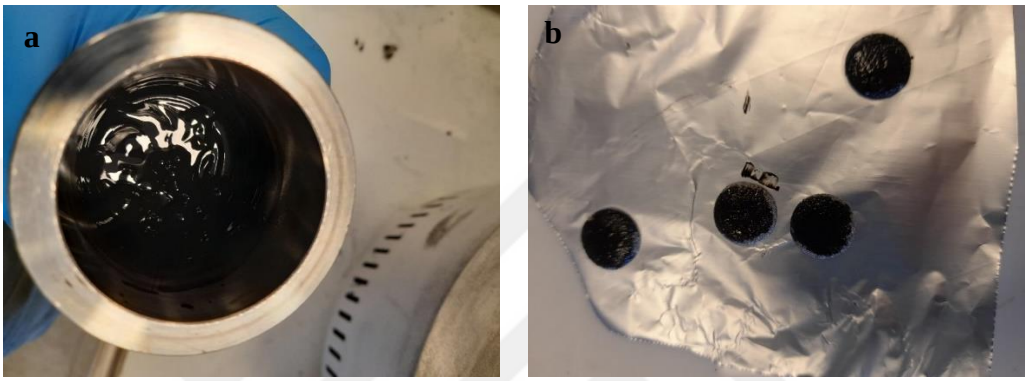


Figure 3-6. Slurry preparation using a) ball mill and b) electrodes

After electrode drying was completed, the custom-made cell was assembled by using a 13mm in diameter and 1.75mm in thickness cathode ($Ni(OH)_2$); 18 mm in diameter and 0.8mm in thickness anode (Cadmium); 18 mm in diameter and 25 microns in thickness separator; and proper amount of electrolyte (6M KOH). The cell is shown schematically in Figure 3-7.

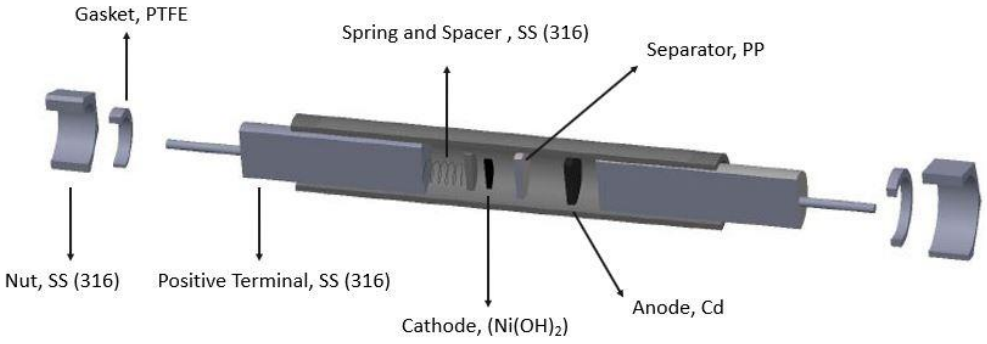


Figure 3-7. Custom made cell

CHAPTER 4

RESULTS AND DISCUSSION

4.1 Structural Characterization

All the samples revealed the diffractogram of α-$Ni(OH)_2$ (ICDD 00-022-0452). Some of the diffractograms are shown in the Figure 4-1, Figure 4-2, Figure 4-3, Figure 4-4 and Figure 4-5. Diffractograms were given in waterfall view for clear visibility. Hence Y-axis is arbitrary

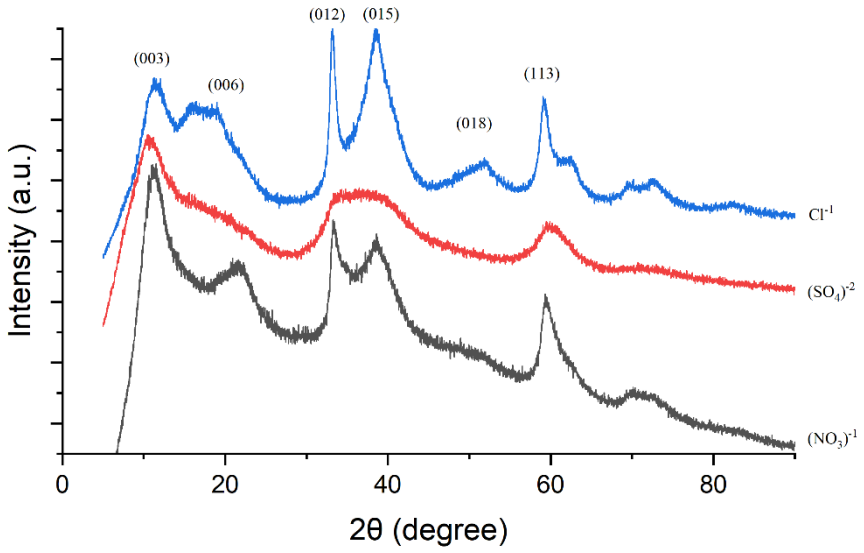


Figure 4-1. Diffractogram of un-doped samples. The blue line at the top represents Cl^{-1}; the middle red lines indicates $(SO_4)^{-2}$ and the bottom black line indicates $(NO_3)^{-1}$

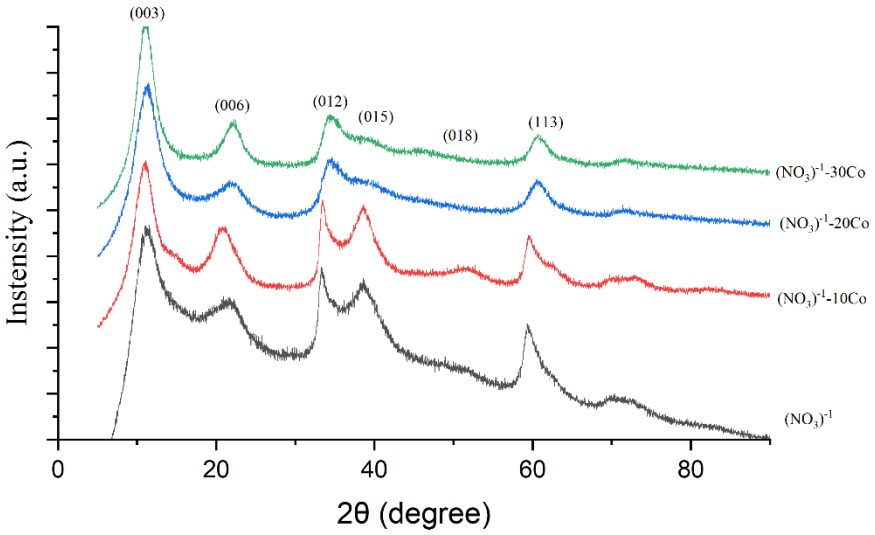


Figure 4-2. Diffractogram of cobalt doped $(NO_3)^{-1}$ based samples. The green line at the top represents 30% doping; blue line under green represents 20% doping and the bottom black line indicates undoped $(NO_3)^{-1}$

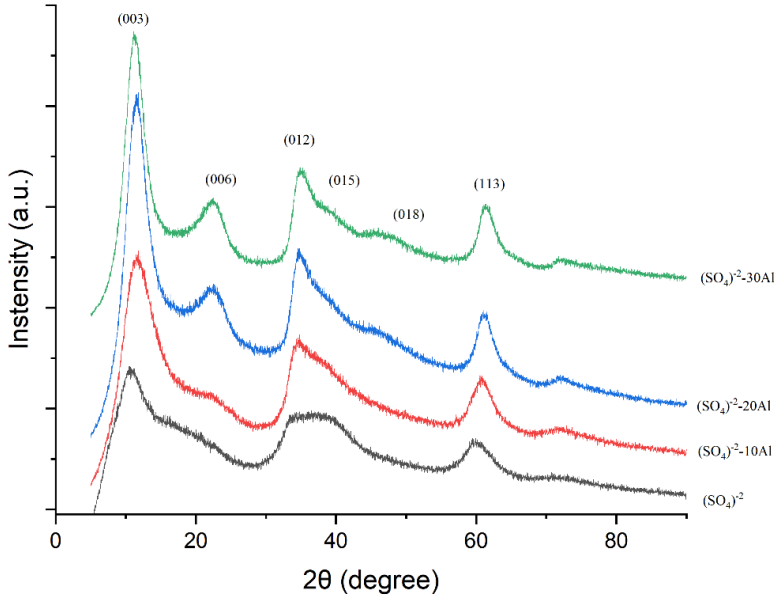


Figure 4-3. Diffractogram of aluminum doped $(SO_4)^{-2}$ based samples. Top green line 30% Al doping; the blue line just below it is 20% Al doping; the bottom black line represents un doped $(SO_4)^{-2}$ sample.

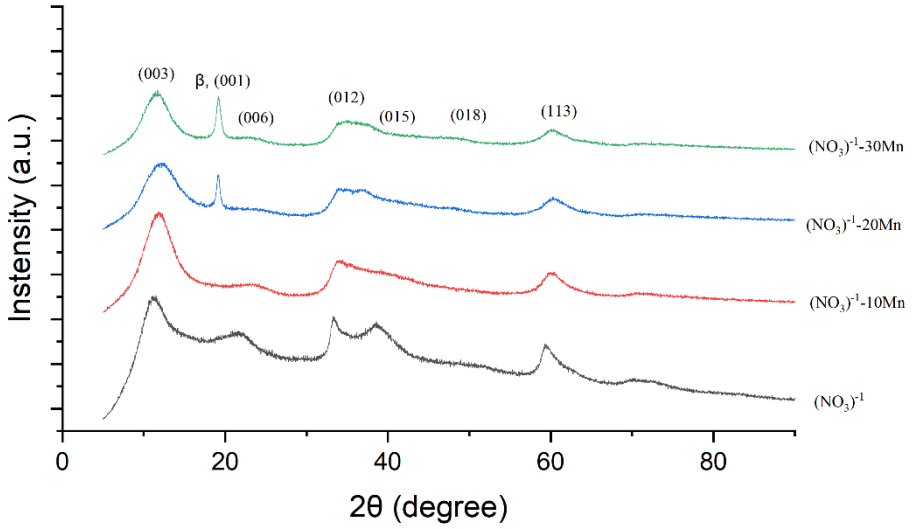


Figure 4-4. Diffractogram of manganese doped $(NO_3)^{-1}$ based samples the green line at the top indicates 30% Mn doping. The line below it shows 20% doping. Peaks belonging to the (001) plane of the Beta phase are seen in both. The bottom line belongs to the sample without any doping.

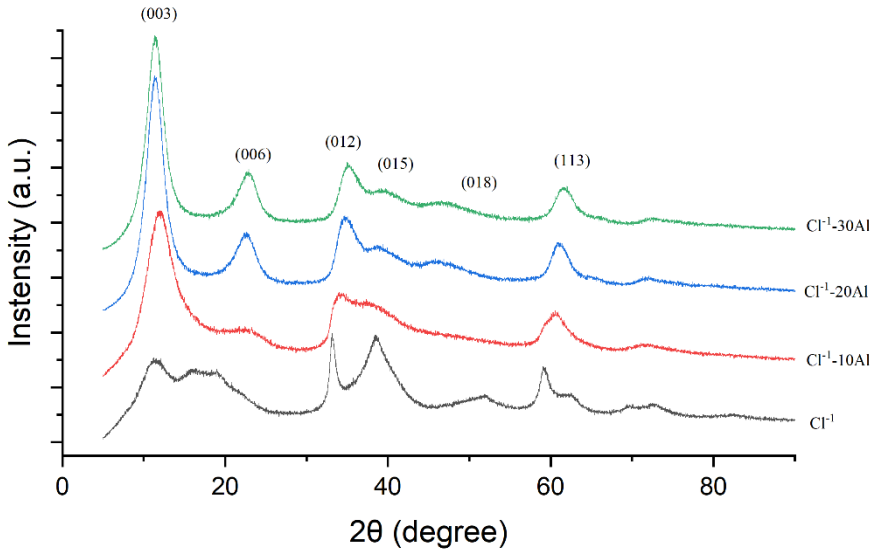


Figure 4-5. Diffractogram of aluminum doped Cl^{-1} based samples. Lines from top to bottom shows 30% 20% and 10% and undoped samples respectively.

Among the samples, there are differences between peak broadening as seen in Table 4-1. Three main reasons cause an increase in peak broadening are as follows:

- Crystal defects
- Grain size reduction
- Mechanical stress

According to XRD results, the highest peak broadening was seen in $(SO_4)^{-2}$ based samples among the un-doped samples. As it is widely known in the literature if the high peak broadening is caused by crystal defects, diffusion coefficient increases, and electrochemical activity increases [35, 36]. But in the case of $(SO_4)^{-2}$ based sample capacity and stability were poorer than Cl^{-1} and $(NO_3)^{-1}$ based samples. It indicates that an increase in peak broadening may be caused by mechanical stress and finer grains.

Regarding doping, as can be seen in Figure 4-2 and Figure 4-4, the intensity of peaks (012) and (015) decreases as the amount of Co and Mn increases. This is a situation known in the literature [37]. In aluminum, there is no such effect. When interpreted by XRD and electrochemical characterization, it was seen that Co and Mn doping reduce peak intensities in different ways. Co creates crystal defect and reduces the intensities of (012) and (015) peaks, while Mn creates interstratified β-$Ni(OH)_2$ and leads to the decrease in intensity of alpha phase peaks. In this context, it can be said that Mn acts as a beta stabilizer. It has been previously stated in the literature that Mn doping leads to the formation of an interstrafied phase [38]. The formation of beta phases within the structure leads to a capacity decrease. The capacity loss can be easily seen by comparing the capacity of $(NO_3)^{-1}$and $(NO_3)^{-1}$-30Mn samples. As the manganese content increases, the peak intensity of the interstratified phases also increases which can be seen from Figure 4-4. The samples which were synthesized with $Ni(SO_4)$ precursors have a higher tendency to form interstratified phase. Peaks of β(001) and β(101) can be easily detected in $(SO_4)^{-2}$-30Mn samples as is seen from Figure 4-6 although β(101) is not detected in $(NO_3)^{-1}$ and Cl^{-1}based samples,

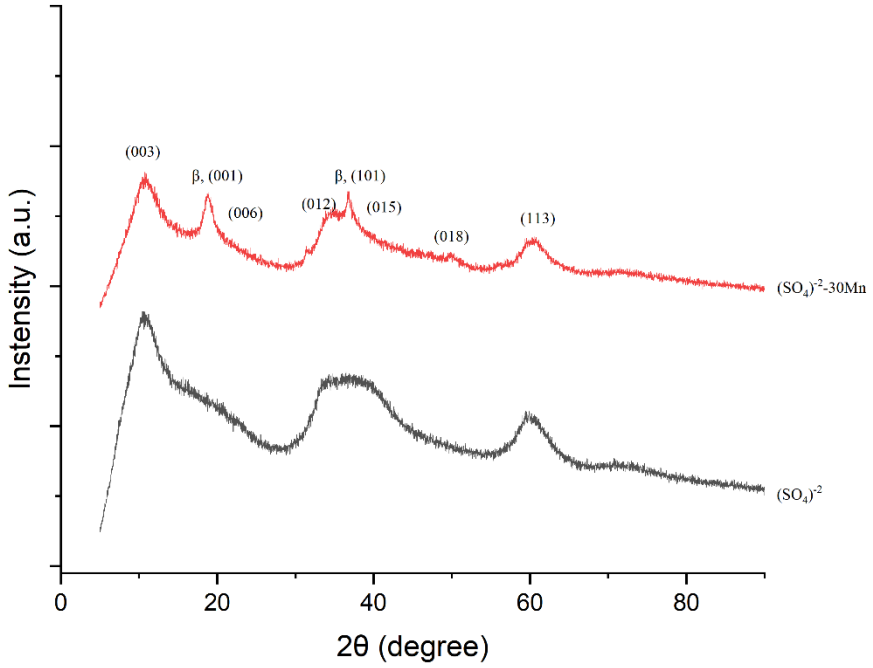


Figure 4-6. Diffractogram of $(SO_4)^{-2}$ and $(SO_4)^{-2}$-30Mn

4.1.1 Stress Analysis

One of the major factors which determines the stability of α-$Ni(OH)_2$ is internal mechanical stress. Mechanical stress of $(NO_3)^{-1}$, $(SO_4)^{-2}$, and Cl^{-1} based samples were compared qualitatively by Williamson-Hall Analysis to investigate intercalated anion-induced mechanical stress. In that analysis, β*cosθ vs. 4sinθ graph is plotted and the slope of the graph gives the stress. Thereby, for qualitative analysis, it can be said that stress is proportional $\frac{\beta_{hkl}}{tan\theta}$. This ratio was calculated for $(NO_3)^{-1}$, $(SO_4)^{-2}$, and Cl^{-1} based samples. The results are given in Table 4-1. To calculate β_{hkl}, $\beta_{instrumental}$ was eliminated from $\beta_{measured}$ according to Equation 13. It can be neglected since $\beta_{instrumental}$ is very small compared to β_{hkl} and $\beta_{measured}$.

$$\beta_{hkl}^2 = \beta_{measured}^2 - \beta_{instrumental}^2 \qquad \text{Equation 13}$$

Table 4-1. Qualitative stress analysis from XRD

	$(NO_3)^{-1}$	$(SO_4)^{-2}$	Cl^{-1}
2θ (degree)	11.51	10.70	12.06
$FWHM_{(200),\ measured}$ (degree)	4.72	6.12	3.76
β_{200} (radians)	0.08	0.11	0.07
$\beta_{instrumental}$ (radians)		$1.92 * 10^{-3}$	
$\frac{\beta_{hkl}}{tan\theta}$ (radians)	0.82	1.14	0.62

$(SO_4)^{-2}$ based samples has higher mechanical stress than others as can be understood from Table 4-1. This is due to the higher ionic radius of $(SO_4)^{-2}$. Furthermore higher mechanical stress causes poor stability.

4.2 Effects of Doping and Precursor on Chargeability and Capacity

The capacities of the samples are shown in Table 4-2

Table 4-2. Dicharge capacities of samples

	$(NO_3)^{-1}$	$(SO_4)^{-2}$	Cl^{-1}
Un doped	281 mAh/g	291 mAh/g	296 mAh/g
10% Co	333 mAh/g	309 mAh/g	342 mAh/g
30% Co	310 mAh/g	290 mAh/g	326 mAh/g
10% Al	313 mAh/g	279 mAh/g	336 mAh/g
30% Al	283 mAh/g	224 mAh/g	-
10% Mn	260 mAh/g	-	-
30% Mn	235 mAh/g	-	259 mAh/g

Although the capacities obtained in the literature vary according to the type and amount of doping, they are generally between 300 mAh/g and 395 mAh/g [39, 40]. As can be seen in Table 4-2, as the amount of doping increases (for all precursors and all dopings), the capacity decreases significantly. The most important thing is that the $(SO_4)^{-2}$-30Mn sample has the lowest discharge capacity. The reason for this may atributed to the formation of the interstratified phase by manganese. Since cobalt and aluminum are not oxidized during the precipitation process, they do not reduce nickel and therefore interstratified phase formation does not occur. In this study, although the experiments with manganese were done in a protective nitrogen atmosphere, it was seen that manganese oxidation could not be hindered completely. Process parameters (such as reactor design and gas flow rate) should be optimized to prevent manganese oxidation and the formation of interstratified phase. Formation of this phase was not observed in 10% Mn doping in this study, but this may be due to the insufficient sensitivity of the XRD.

Chargeability is one of the most important factors that affect the capacity of a battery. In nickel-based batteries, chargeability problems can occur because E_{OER} and E_{OX} are very close to each other. It is necessary to increase the difference between E_{OER} and E_{OX} as much as possible to increase the capacity. Among the doping materials, cobalt and manganese make E_{OX} more negative, while in the case of aluminum doping, the oxidation peak shifts to the positive region. Accordingly, as it shifts to the positive region, oxygen evolution, which is a side reaction, increases and chargeability becomes poor. This was observed in all precursors and doping levels. Figure 4-7 shows how doping changes the oxidation potentials in $(NO_3)^{-1}$ and nitrate-based 30% doping materials. The numerical data of this Cyclic Voltammogram (CV) are given in Table 4-3. As it can be seen from Figure 4-7, cobalt and manganese doping shifts the oxidation peak to the more negative region and increases the difference between the oxygen evolution and electrode oxidation potential. On the other hand, aluminum reduces the difference between E_{OER} and E_{OX} by shifting the oxidation peak to the positive region. This indicates that the aluminum doped nickel

hydroxide samples have a higher driving force for oxygen evolution compared to the other samples.

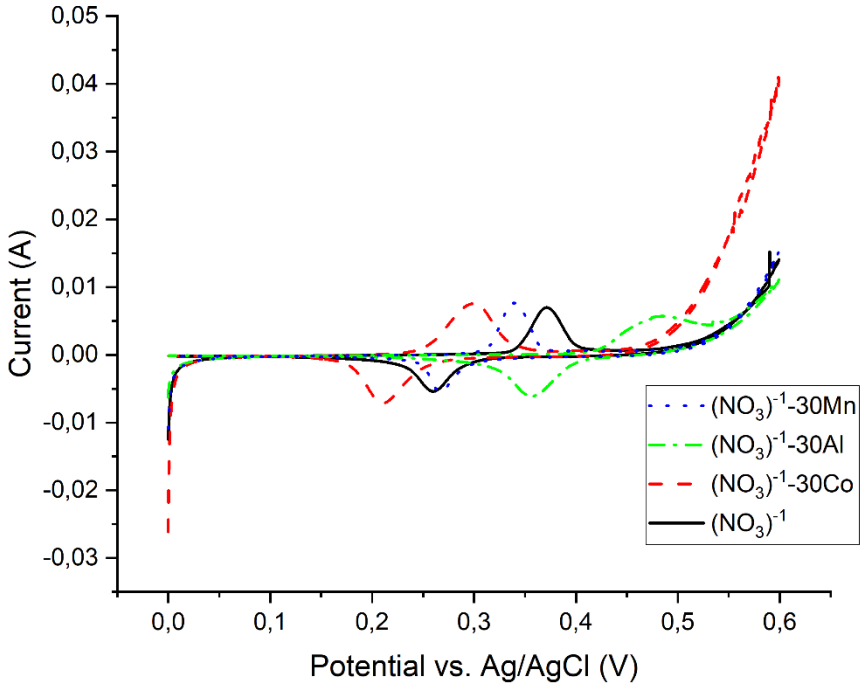


Figure 4-7. CV of $(NO_3)^{-1}$ based %30 doped samples. Scan rate 0.25mv/S

Table 4-3. Peak positions $(NO_3)^{-1}$ based %30 doped samples. Scan rate is 0.25mV/s

Material	E_{OX}	E_{OER}	E_{OER}-E_{OX}
$(NO_3)^{-1}$	371	479	108
$(NO_3)^{-1}$-30Co	301	453	152
$(NO_3)^{-1}$-30Al	486	546	60
$(NO_3)^{-1}$-30Mn	339	492	153

Especially in the samples with 30% Al doped and synthesized with nitrate and sulfate, the capacity decreases considerably. Since the aluminum doping reduces the E_{OER}-E_{OX} difference, the electrode oxidation potential becomes higher than the

oxygen evolution potential and after a certain point, the electrode becomes non-chargeable. Figure 4-8 shows the CV of 10% Al doped materials that were synthesized with $(NO_3)^{-1}$, $(SO_4)^{-2}$, and Cl^{-1} precursors. It is seen that oxidation potential and starting point of oxygen evolution potentials are very close to each other (compare to Co and Mn doped samples in Figure 4-7). Effect of oxygen evolution can be seen more clearly in $(SO_4)^{-2}$-30Al, the sample that has the lowest capacity that is obtained in this study. In this sample, the oxidation peak and the oxygen evolution voltage are very close to each other, even indistinguishable. CV of this sample is shown in Figure 4-9.

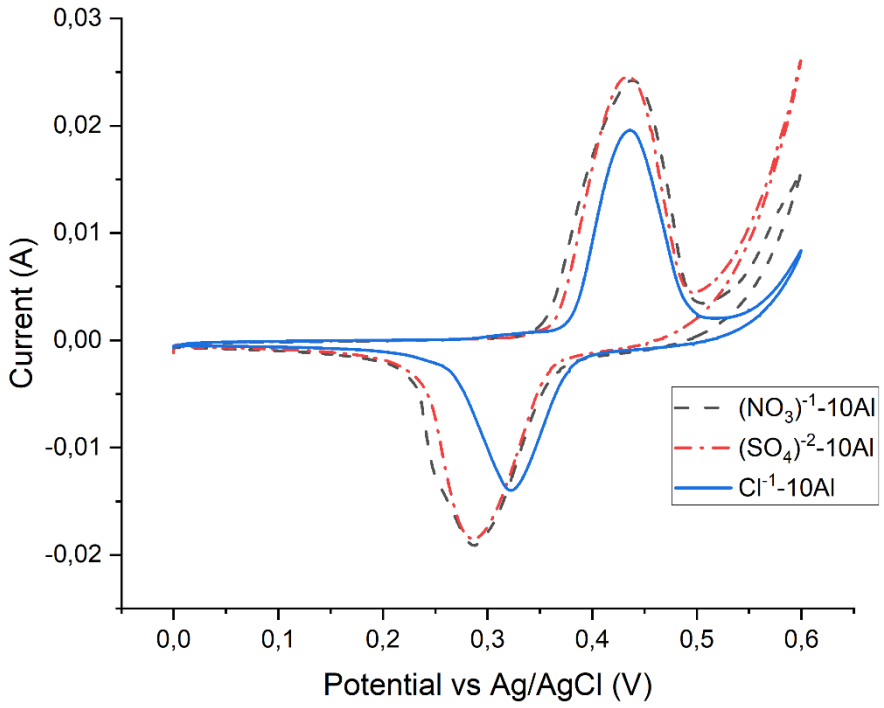


Figure 4-8. CV of %10 Al doped samples. Scan rate 0.25 mV/s

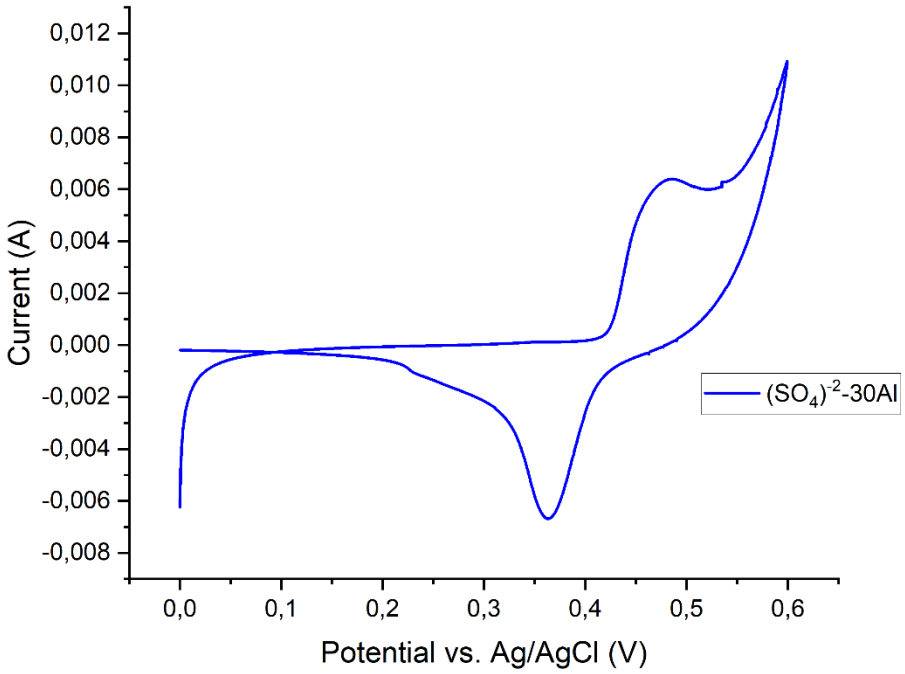


Figure 4-9. CV of $(SO_4)^{-2}$-30Al. Scan rate 0.25 mV/s

As it is seen in Figure 4-8, the sample that oxygen evolution starts the fastest is the sample synthesized with sulfate, and the latest one is the sample synthesized with Cl^{-1}. This shows why the samples that were synthesized with Cl^{-1}have the highest capacity. This is not only valid for aluminum doping but also other types of doping. Among the precursors in this study, all samples synthesized with chlorine, show higher capacity compared to other precursors since oxygen evolution potential is highest in chlorine based samples.

A high amount of oxygen evolution means that some portion of the applied current is consumed by oxygen evolution. Thereby, charge acceptance and discharge capacity decrease. This problem becomes very critical in fast charging. Nickel-based batteries do not have a constant voltage charge sequence (unlike lithium-ion batteries) due to the very high self-discharge at the end of the state of charge.

Therefore, nickel-based batteries are charged with the only constant current charging protocol. The commercial approach generally used in this protocol is to cut off the charging process at the point where the cell voltage starts to drop. The reason for the voltage drop at the end of the charge is the oxygen evolution that occurs at the cathode and it is known that the evolved oxygen oxidizes the anode, thereby voltage of the cell decreases. If the oxygen evolution begins early, this causes premature charging cut-off before the cell is completely charged. In summary, the dopant that increases the oxygen evolution is not suitable for high rate charging. Additionally, oxygen evolution causes premature degradation of electrolyte and high internal pressure of cell (safety problems).

Compared to undoped samples, Al and Co doped samples have higher capacity while Mn doping decreases the capacity. The situation of Mn was explained before (interstratified phase formation). $(SO_4)^{-2}$based aluminum samples have very low capacity and it can be explained by the chargeability problem. Both Al doping and $(SO_4)^{-2}$precursor decrease the E_{OER}- E_{OX}. In other words, a combination of $(SO_4)^{-2}$-Al is the worst case for chargeability. In the case of Co and Al doping, the increase in capacity can be explained by impedance and diffusion coefficient. According to the results, doping with these elements decreases the impedance and increases the diffusion coefficient. Figure 4-10 shows the decrease in EIS in the case of Co doping. The findings obtained in this area are also compatible with the literature [41].

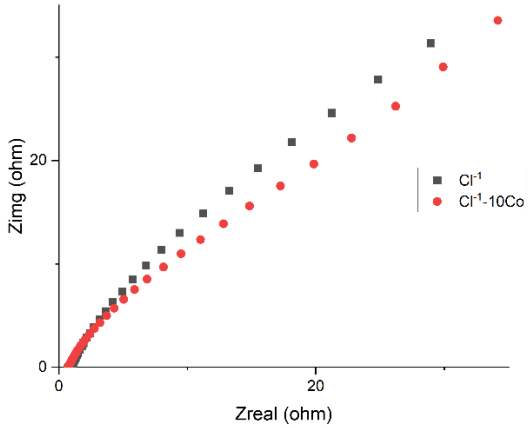


Figure 4-10. EIS of Cl^{-1} and Cl^{-1}-10Co

Another important parameter for active mass utilization is the hydrogen diffusion coefficient. The diffusion coefficient was calculated by the Randles-Sevcik equation which is shown in Equation 14 [33].

$$I_a = 2.69 * 10^5 * n^{\frac{3}{2}} * A * D^{\frac{1}{2}} * C_0 * V^{1/2} \qquad \text{Equation 14}$$

In the above equation I_a anodic peak current; n, number of the electron that is involved in reaction; A, surface are (of working electrode); C_0, the composition of hydrogen in the material; D, diffusion coefficient; V is scan rate (in CV). For qualitative analysis, I_a vs. square root of scan rate graph is plotting and slope of that graphic is used to compare diffusion coefficient of samples. “Ia vs. Square roof of can rate” graph was plotted for $(NO_3)^{-1}$, and $(NO_3)^{-1}$-30Co, $(NO_3)^{-1}$-30Al, $(NO_3)^{-1}$-30Mn as seen in Figure 4-11

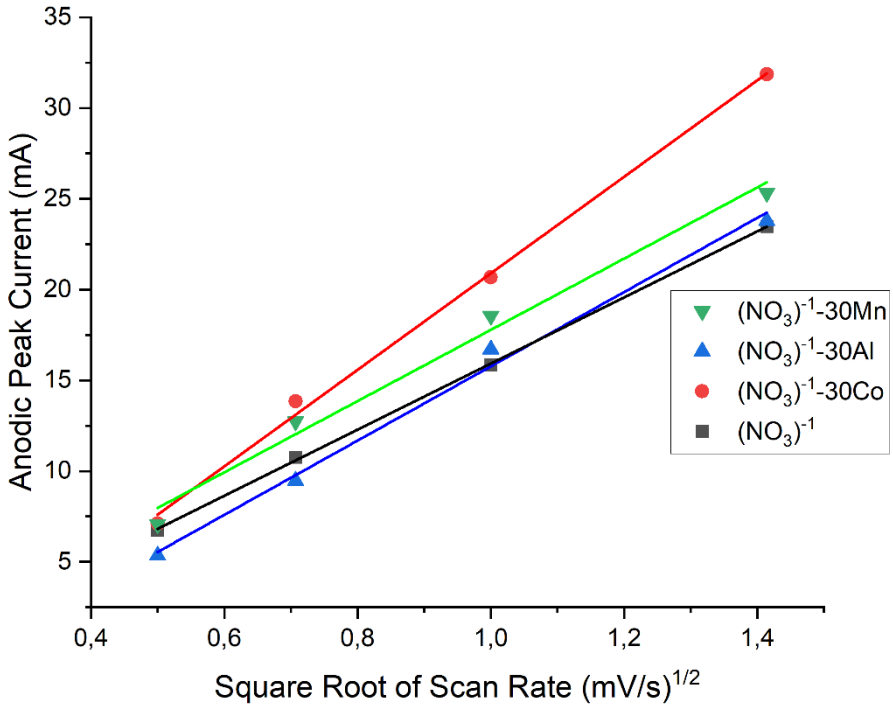


Figure 4-11. I_a vs. sqr(Scan Rate) for $(NO_3)^{-1}$ based samples

Table 4-4. Slope of the I_a vs. sqr(Scan Rate) graph for $(NO_3)^{-1}$ based samples

	$(NO_3)^{-1}$	$(NO_3)^{-1}$-30Co	$(NO_3)^{-1}$-30Al	$(NO_3)^{-1}$-30Mn
Slope (mA/(mV/s)$^{1/2}$)	18.20± 0.21	26.58 ± 0.94	20.45 ± 1.37	19.61 ± 1.54

Qingsheng et al. [42] found this slope value between 52 mA/(mV/s)$^{1/2}$ and 72 mA/(mV/s)$^{1/2}$ for different materials. The lower values in this study may be due to the electrode thickness and the composition of the active material slurry as well as from the material itself. Since it is difficult to substitute the composition and real surface area values in the Randles-Sevcik equation, the diffusion coefficient could not be calculated directly, comparisons were made qualitatively. Doping increases the diffusion coefficient as is seen in Figure 4-11 and Table 4-4. The higher capacity of doped materials can be explained by a higher diffusion rate. The highest increase

in diffusion coefficient is seen in Co doping, due to this reason, the highest capacity increase is observed in Co doping (in addition to diffusion rate Co doping also decreases impedance, Figure 4-10). The number of electrons that are involved in the redox reaction can be analyzed to demonstrate the capacity increase is caused by a higher diffusion rate and a lower impedance. Although the number of electrons in un-doped samples is higher than the doped samples, un-doped samples have a lower capacity than the doped ones. The number of electrons that are involved in the redox reaction was calculated by Shain Equation which is shown in Equation 15.

$$E_{OX} - E_{\frac{OX}{2}} = \frac{1.857 * R * T}{\alpha * n * F} \qquad \text{Equation 15}$$

E_{OX} is anodic peak potential (V); $E_{OER/2}$, anodic peak potential at half height of anodic peak current after non-faradaic current subtraction (V); R, gas constant ($J*K^{-1}*M^{-1}$); T, temperature (K); α, transfer coefficient (it is taken as 0.5 and unitless); F, Faraday constant (C/M). The number of electrons involved in the redox reaction was calculated for some of the samples are given in Table 4-5.

Table 4-5. Number of electrons that are involved in the reaction

	E_{OX} (V)	$E_{OX/2}$ (V)	T (ºC)	#of e^- involved in reaction
$(NO_3)^{-1}$	0.42	0.37	20	1.96
$(SO_4)^{-2}$	0.41	0.36	18	1.99
Cl^{-1}	0.44	0.39	20	1.80
$(NO_3)^{-1}$-10Co	0.40	0.35	20	1.65
$(NO_3)^{-1}$-10Al	0.46	0.39	20	1.49
$(SO_4)^{-2}$-10Co	0.41	0.35	20	1.51
$(SO_4)^{-2}$-20Co	0.41	0.34	21	1.34
$(SO_4)^{-2}$-10Al	0.46	0.40	20	1.72
$(SO_4)^{-2}$-20Al	0.54	0.47	20	1.29
Cl^{-1}-30Co	0.37	0.33	22	1.67

Doping increases the capacity of material but as the amount of doping increases capacity decreases due to a decrease in active mass. This is all right for Co but not an adequate explanation for Al and Mn doping. As it is stated before, increasing amount of Al doping causes chargeability problems, and Mn yields the formation of an interstratified phase.

The capacity of energy storage materials (in terms of mAh/g) is a major parameter that determines the performance of material but energy density (in terms of Wh/kg) should be considered also. Higher discharge voltage gives higher energy density. Accordingly, some of the energy storage studies focus on increasing discharge voltage. It was found that the type and level of doping affect discharge voltage of α-$Ni(OH)_2$ considerably in this study. Theoretically, any doping which decreases the E_{OX} shall cause a decrease in voltage. Discharge curves of $(NO_3)^{-1}$-30Al, $(NO_3)^{-1}$-30Co, and $(NO_3)^{-1}$-30Mn are shown in Figure 4-12.

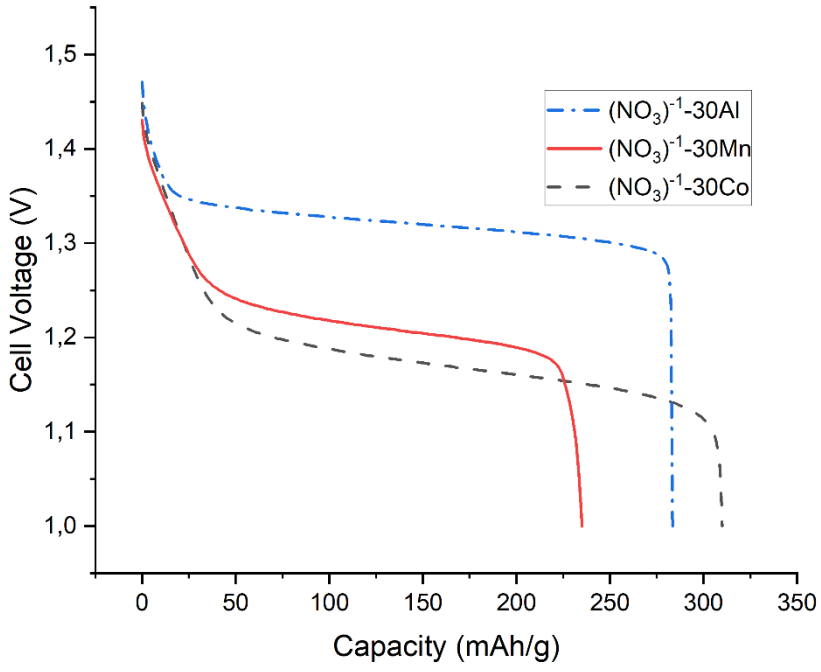


Figure 4-12. Discharge curve of $(NO_3)^{-1}$ based samples

Average discharge voltage of the samples in Figure 4-12 is decreasing in order $(NO_3)^{-1}$-30Al (1.32V) > $(NO_3)^{-1}$-30Mn (1.22V) > $(NO_3)^{-1}$-30Co (1.19V). The voltage profile of these samples verifies the assumption that higher E_{OX} yields higher discharge voltage (Table 9 shows E_{OX} these samples). Another reason for the differences in discharge voltage is the impedance of the samples. To understand whether voltage differences are caused by impedance differences, EIS of $(NO_3)^{-1}$ based samples were compared and it is found that the Nyquist plot of these samples which is shown in Figure 4-13 almost the same. Even, Co doped sample has lower impedance than Al doped sample although Al doped sample has a higher discharge voltage. Thus it is reasonable to say that voltage difference is caused by the effects of doping on E_{OX}, not impedance of samples.

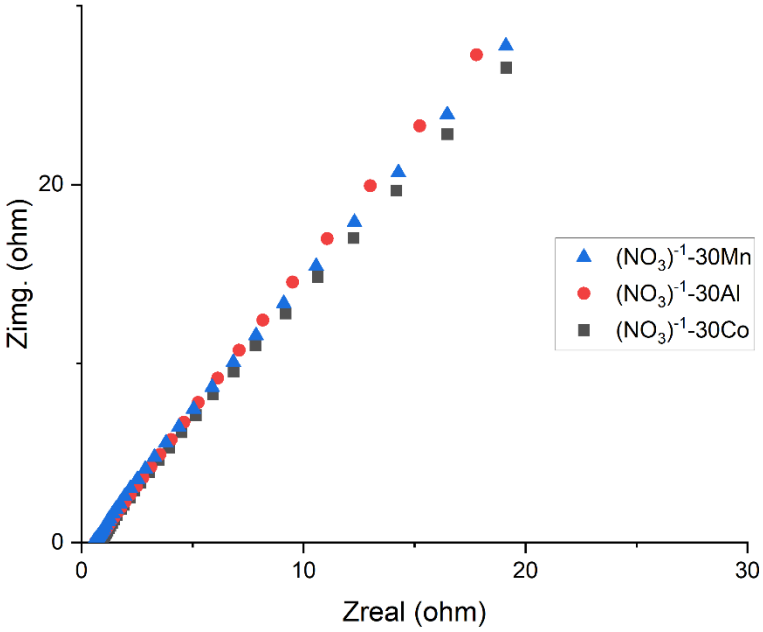


Figure 4-13. EIS of $(NO_3)^{-1}$ based samples

It must be noted that, although higher voltage raises the energy density of the battery, higher voltage gives cause for higher self-discharge and chargeability problems due to higher oxygen evolution rate.

4.3 Effects of Doping and Precursor on Self-Discharge

To measure the self-discharge rate, the following procedure was implemented.

1. The electrode was prepared in accordance with the steps explained in the Experimental Procedure
2. The cell was assembled by using cadmium anode
3. The activation process was done (low rate charging for 3 cycles)
4. The cell was charged and discharged until capacity is stabilized
5. Fully charged cell was aged at 60 °C for 24 hours
6. It was waited at room temperature for 1 hour to cool down
7. It was discharged
8. Self-discharged was calculated by the ratio of the capacity in step 7 and step 4

The discharge profile of a typical self-discharge measurement can be seen in Figure 4-14 and Table 4-6 shows the self-discharge rate of samples.

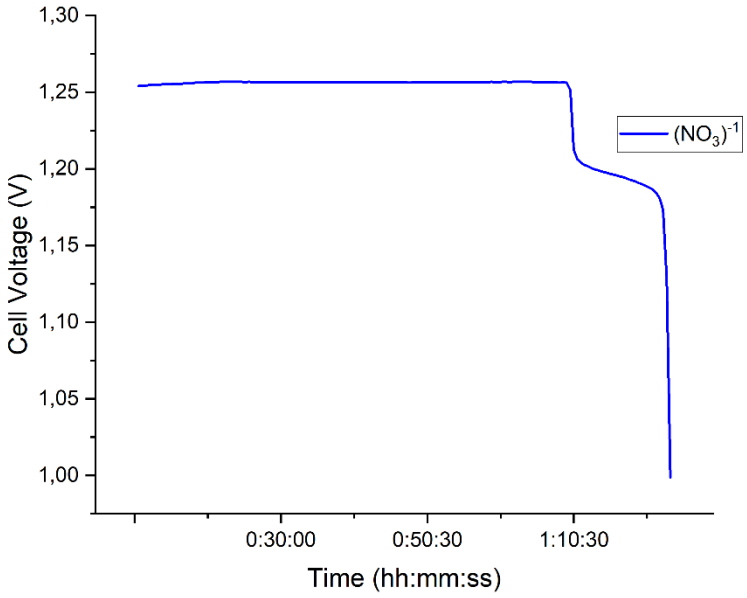


Figure 4-14. Self-discharge measurement of $(NO_3)^{-1}$

Table 4-6. Self-discharge rate of samples

Sample	Self Discharge	Sample	Self-Discharge
$(NO_3)^{-1}$	67%	$(NO_3)^{-1}$-10Mn	64%
$(SO_4)^{-2}$	100%	$(SO_4)^{-2}$-30Co	90%
Cl^{-1}	71%	$(SO_4)^{-2}$-20Al	95%
$(NO_3)^{-1}$-20Co	62%	$(SO_4)^{-2}$-30Al	100%
$(NO_3)^{-1}$-30Co	37%	Cl^{-1}-10Co	60%
$(NO_3)^{-1}$-20Al	100%	Cl^{-1}-30Co	57%
$(NO_3)^{-1}$-30Al	100%	Cl^{-1}-30Al	100%

It is seen that any dopant or precursor that increases the E_{OER}-E_{OX}, yields a lower self-discharge rate. Co and Mn doped samples have a lower self-discharge rate than Al doped samples. It calls attention to the relation between self-discharge and oxygen evolution. Since Al doped samples have higher E_{OX}, at the end of charging the cell voltage of these samples is higher than Mn and Co doped samples. Higher E_{OX} accelerates the electrolysis of electrolyte and oxygen evolution (Equation 4) when the cell was kept charged state. In a charged cell, oxygen evolution is an anodic process, and electron is released during that process according to Equation 15. The released electron is accepted by NiOOH and it is reduced to $Ni(OH)_2$ as shown in Equation 16 and it is the major self-discharge reaction.

$$4OH^- \rightarrow O_2 + 2H_2O + 4e^- \qquad \text{Equation 15}$$

$$NiOOH + H_2O + e^- \rightarrow Ni(OH)_2 + OH^- \qquad \text{Equation 16}$$

Since Mn and Co doping decrease E_{OX}, it shows better self-discharge performance than Al doped and un-doped samples. If the effects of Mn and Co doping are compared to each other, it can be said that Mn doping shows better self-discharge characteristics ($(NO_3)^{-1}$-10Mn has the same self-discharge rate as $(NO_3)^{-1}$-20Co although it has a lower amount of dopant). It can be explained in two ways:

1. Mn doping does not change E_{OER} while Co doping decreases it so oxygen evolution requires more energy in Co doping.

2. Mn doping yields the formation of interstratified β-$Ni(OH)_2$ and it is known that the beta phase has lower catalytic activity for oxygen evolution

In the case of precursors, it is not convenient to explain self-discharge performance by only oxygen evolution kinetics. E_{OER}-E_{OX} is almost the same for Cl^{-1} (E_{OER}-E_{OX}=102 mV) and $(NO_3)^{-1}$ (E_{OER}-E_{OX}=109 mV). Un-doped and doped chlorine based samples have a higher self-discharge rate than un-doped and doped $(NO_3)^{-1}$ based samples. Considerably high self-discharge of Cl^{-1} based samples can be explained by their high electrochemical activity. Since Cl^{-1} based samples have a higher diffusion coefficient than $(NO_3)^{-1}$ based samples, they have higher activity and thereby higher self-discharge. Self-discharge reaction (in Equation 16) requires diffusion of species [16]. The diffusion coefficient of un-doped $(NO_3)^{-1}$ and Cl^{-1} is compared in Figure 4-15 qualitatively, Cl^{-1}has a higher slope.

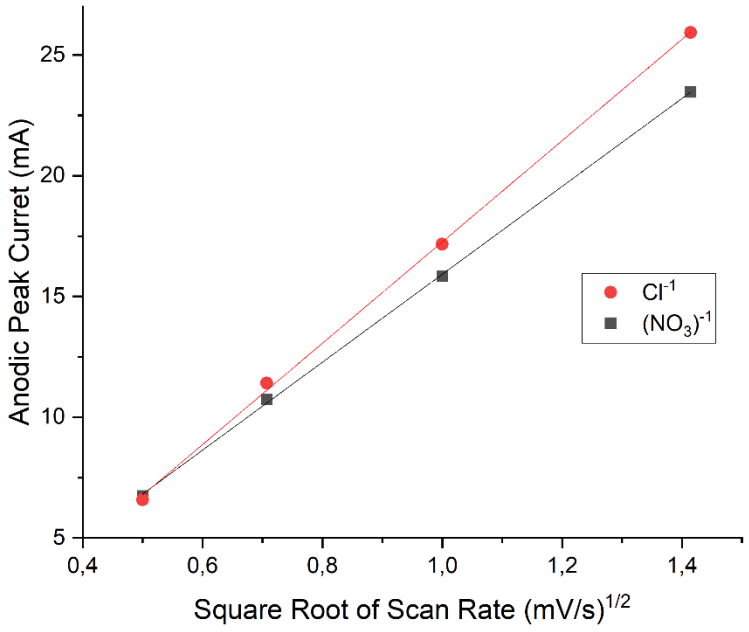


Figure 4-15. Ia vs. sqr(scan rate) plot of $(NO_3)^{-1}$ and Cl^{-1}

4.4 Morphological Characterization and Tap Density

The tap density of some of the samples is given in Table 4-7. EDS results are in Table 4-8 and SEM images in Figure 4-16.

Table 4-7. Tap density of samples

Sample	Tap Density (g/cm^3)	Sample	Tap Density(g/cm^3)
$(NO_3)^{-1}$	1.18	$(NO_3)^{-1}$-30Mn	0.56
$(SO_4)^{-2}$	0.61	$(SO_4)^{-2}$-30Co	0.76
Cl^{-1}	1.43	$(SO_4)^{-2}$-10Al	0.50
$(NO_3)^{-1}$-10Co	1.18	$(SO_4)^{-2}$-30Al	0.86
$(NO_3)^{-1}$-30Co	1.19	$(SO_4)^{-2}$-30Mn	0.39
$(NO_3)^{-1}$-10Al	0.53	Cl^{-1}-10Al	0.56
$(NO_3)^{-1}$-30Al	1.53	Cl^{-1}-30Al	1.32
$(NO_3)^{-1}$-10Mn	0.52	Cl^{-1}-10Mn	0.51
$(NO_3)^{-1}$-20Mn	0.53	Cl^{-1}-30Mn	0.66

Table 4-8. EDS results of samples

Sample	Target Stoichiometry (M_{nickel}/M_{dopant})	EDS Result (M_{nickel}/M_{dopant})
$(NO_3)^{-1}$-30Co	Ni/Co=2.33	Ni/Co=2.33
$(NO_3)^{-1}$-30Al	Ni/Al=2.33	Ni/Al=2.41
$(NO_3)^{-1}$-30Mn	Ni/Mn=2.33	Ni/Mn=2.61
$(SO_4)^{-2}$-30Al	Ni/Al=2.33	Ni/Al=2.35
Cl^{-1}-10Co	Ni/Co=9.00	Ni/Co=9.13
Cl^{-1}-30Al	Ni/Al=2.33	Ni/Al=2.59

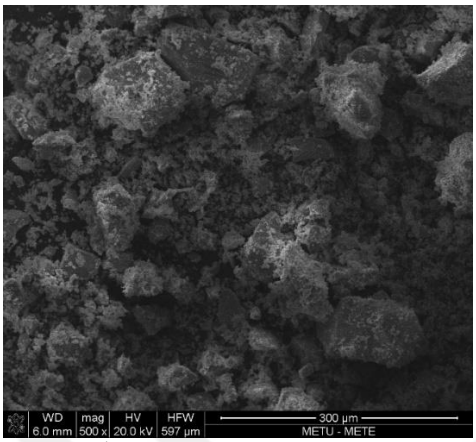
Among the precursors, $(SO_4)^{-2}$ has the lowest tap density. Since d-spacing affects the tap density, the difference in tap density of precursors can be explained by the type of intercalated anion. Interlayer spacing of samples was analyzed by peak position of (003) plane, 2θ values of some of the samples are shown in Table 4-9. According

to Bragg's law, interlayer spacing increases as the diffraction peak shifts towards to lower angle.

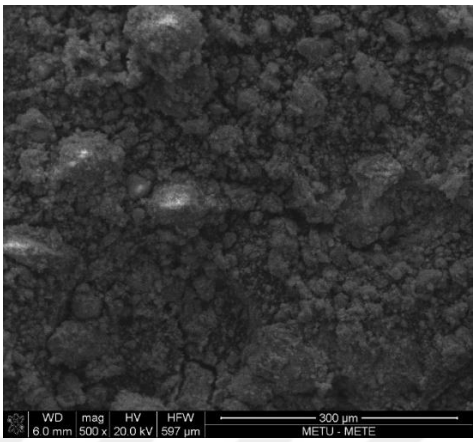
Table 4-9. 2θ Diffraction angle of samples

Sample	2θ (degree)
$(NO_3)^{-1}$	10.98
$(SO_4)^{-2}$	10.43
Cl^{-1}	11.53
$(NO_3)^{-1}$-30Co	10.96
SO_4-30Co	10.86
$(NO_3)^{-1}$-30Al	11.17

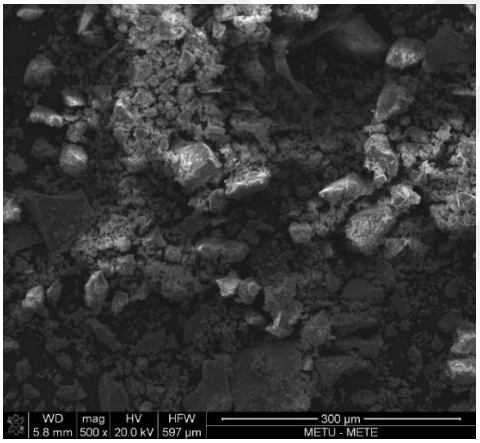
The sample which has the lowest interlayer spacing, Cl^{-1}, has the highest tap density as expected. Since Co has an atomic radius that is very close to Ni, doping with Co does not change 2θ of $(NO_3)^{-1}$. Unlike $(NO_3)^{-1}$, Co doping decreases the interlayer spacing of $(SO_4)^{-2}$ samples. As a result of this, the tap density of $(SO_4)^{-2}$-30CO is higher than un-doped $(SO_4)^{-2}$. In the studies in the literature, the tap density value of α-$Ni(OH)_2$ generally varies between 0.75 g/cm^3 and 1.4 g/cm^3 [43,44], but it is also seen that the tap density value can be increased up to 1.9 g/cm^3 [45].



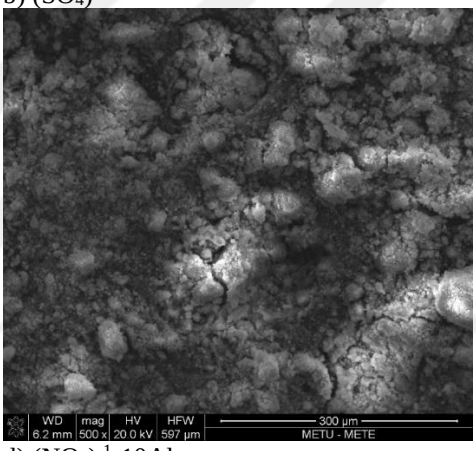
a) $(NO_3)^{-1}$



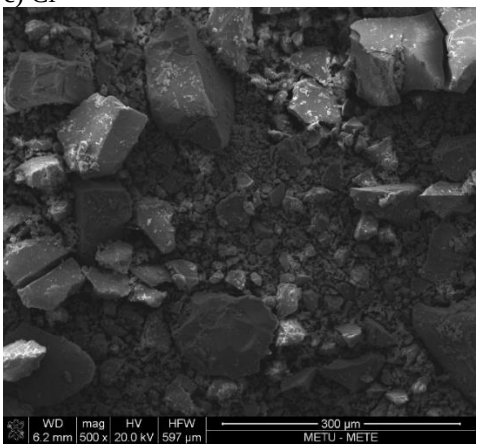
b) $(SO_4)^{-2}$



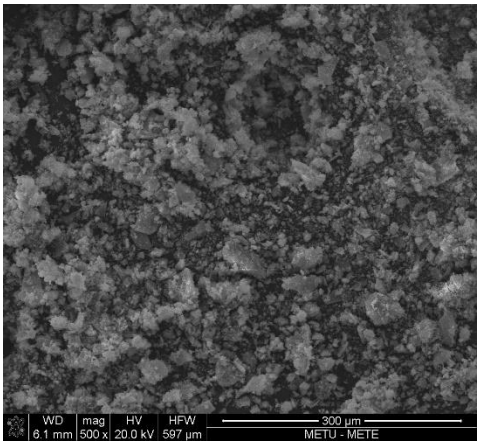
c) Cl^{-1}



d) $(NO_3)^{-1}$-10Al



e) $(NO_3)^{-1}$-30Al



e) $(NO_3)^{-1}$-30Mn

Figure 4-16. SEM images of samples

The effects of aluminum on tap density are remarkable. A low level of Al doping decreases the tap density as is reported in the literature. In this study, it was found that the high doping level of Al enhanced the tap density due to precipitation characteristics. Unlike other doping materials, the precipitation reaction starts early when aluminum is used. Therefore, the first precipitated particles have enough time to grow. As a result of this, some portions of the particles get bigger while the rest of the particles (precipitated towards the end of the reaction) could not find enough time to get grown up. This type of particle distribution is known as bimodal distribution and it increases the tap density of a powder. In Figure 26e, it can be seen that particles of $(NO_3)^{-1}$-30Al look bimodal. Although this type of particle size distribution is beneficial for tap density, it is problematic for side reactions and cycle life due to uncontrolled surface area. One of the samples with the lowest tap density is $(NO_3)^{-1}$-30Mn. This material has a smaller particle size and the shape of the particles are not spherical as is seen in Figure 26f. That is why the tap density of that sample is very low.

4.5 Effects of Precursor and Doping on Stability

The samples that were synthesized with $(SO_4)^{-2}$ have poor stability than that of samples synthesized from $(NO_3)^{-1}$ and $(Cl)^{-1}$. The stability curve of those samples is shown in Figure 4-17. The best explanation for the poor stability of $(SO_4)^{-2}$is internal mechanical stress. Since sulfate ions are bigger than Cl^{-1} and NO^{-}_3 ions, it creates more mechanical stress in the lattice. Mechanical stress analysis was done by the Williamson-Hall approach and it was explained in Section 4.1.1. Stress causes particle cracking that is why material with high internal stress has poor cycle life. Because of the higher mechanical stress in $(SO_4)^{-2}$, the capacity is constantly decreasing, unlike Cl^{-1} and $(NO_3)^{-1}$.

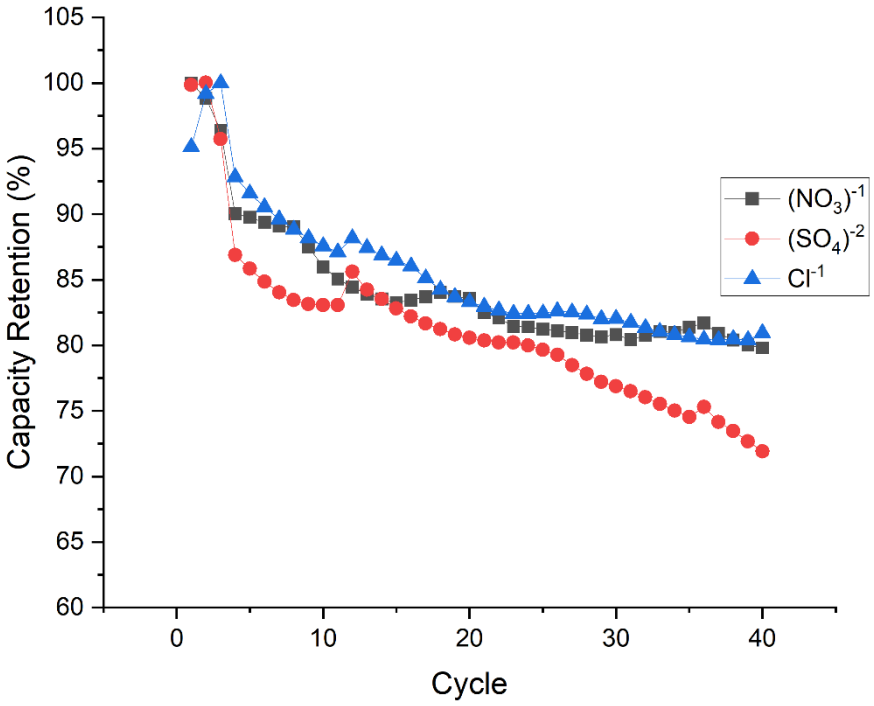


Figure 4-17. Stability curve of un-doped samples

Co doping increases stability considerably. Substitution of Co^{+3} creates an excess positive charge in the lattice, thus anions bond strongly to the lattice. Figure 4-18 shows the effects of Co doping on stability.

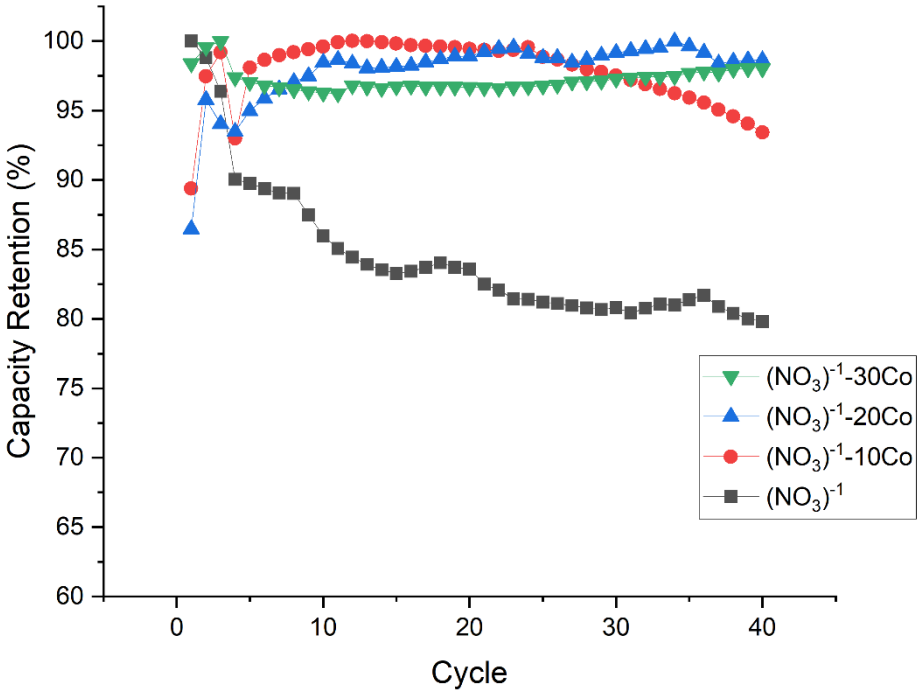


Figure 4-18. Effects of Co doping on stability. (100 mA/g for 3 cycles, rest of the cycles 400mA/g)

10% Co doping increases stability considerably but a higher doping level does not change stability notably. The fact that a low amount of cobalt doping is enough is seen in other precursors. Figure 4-19 shows the effects of Co doping on the stability of $(SO_4)^{-2}$. This figure is a piece of evidence that there are no differences between 20% and 30% of Co doping in terms of stability. Aluminum also increases the stability of α-$Ni(OH)_2$ but it is a necessity to dope a higher amount of aluminum to obtain stability. In Figure 4-20 this phenomenon can be seen, to obtain stability 20% of Al doping is not enough at least 30% is required.

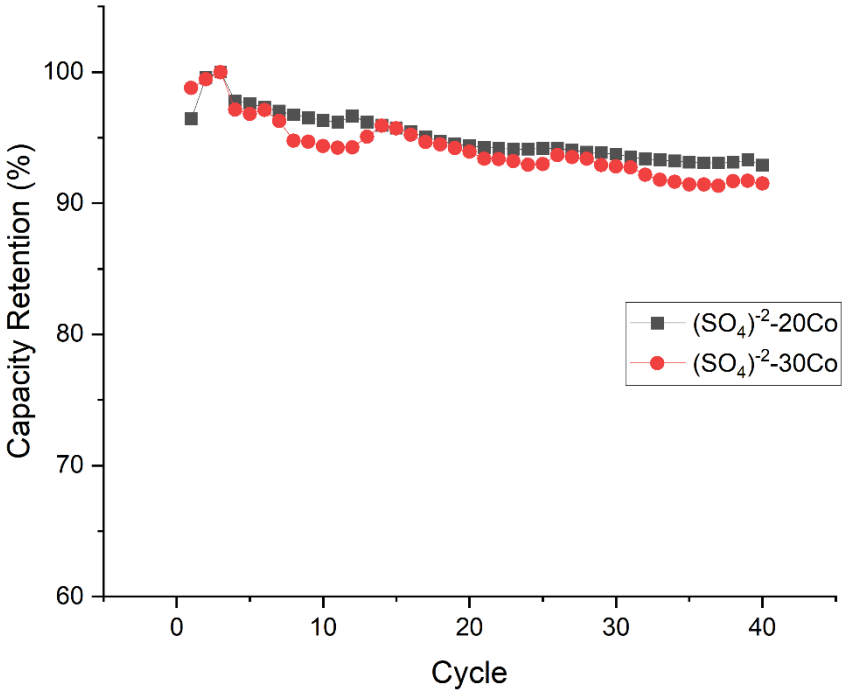


Figure 4-19. Effect of Co doping on the stability of $(SO_4)^{-2}$ based sample (100 mA/g for 3 cycles, rest of the cycles 400mA/g)

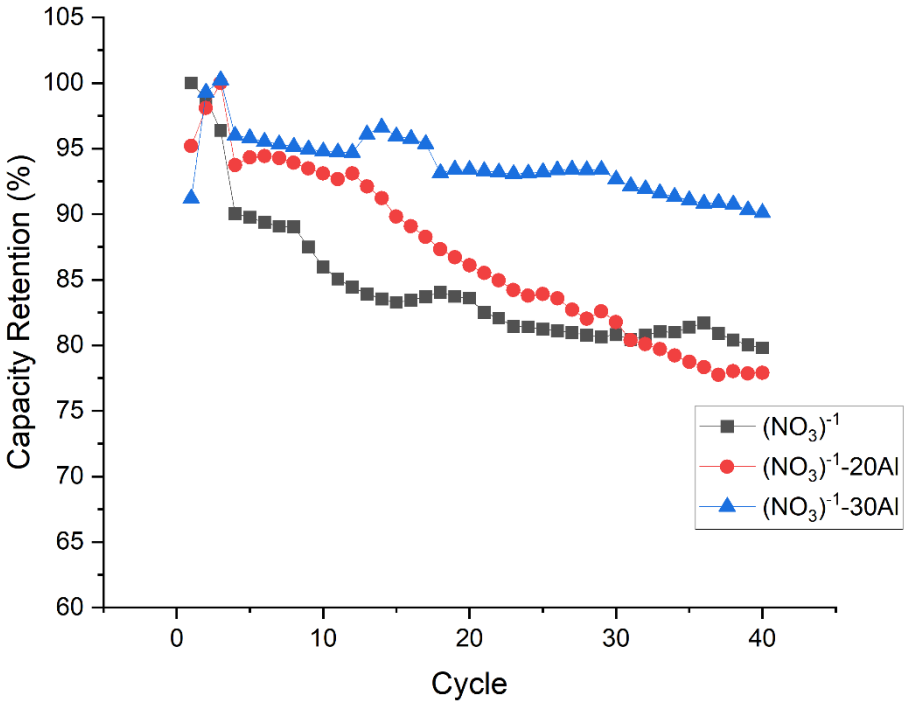


Figure 4-20. Effect of Al doping on the stability of $(NO_3)^{-1}$ based sample (100 mA/g for 3 cycles, rest of the cycles 400mA/g)

In the case of Al doped $(SO_4)^{-2}$ based samples, there is an interesting point. It seems Al doping works for stability but capacity begins to fall rapidly after approximately 15 cycles. Even, after 35 cycles capacity retention of doped sample becomes lower than un-doped samples. This situation indicates electrolyte degradation. It is expected because as it is explained before $(SO_4)^{-2}$-Al is the worst combination since when two of them are combined oxygen evolution rate becomes the highest level. Higher oxygen evolution rate yields premature degradation (low coulombic efficiency) and poor cycle life. Cycle life of $(SO_4)^{-2}$-Al can be seen in Figure 4-21

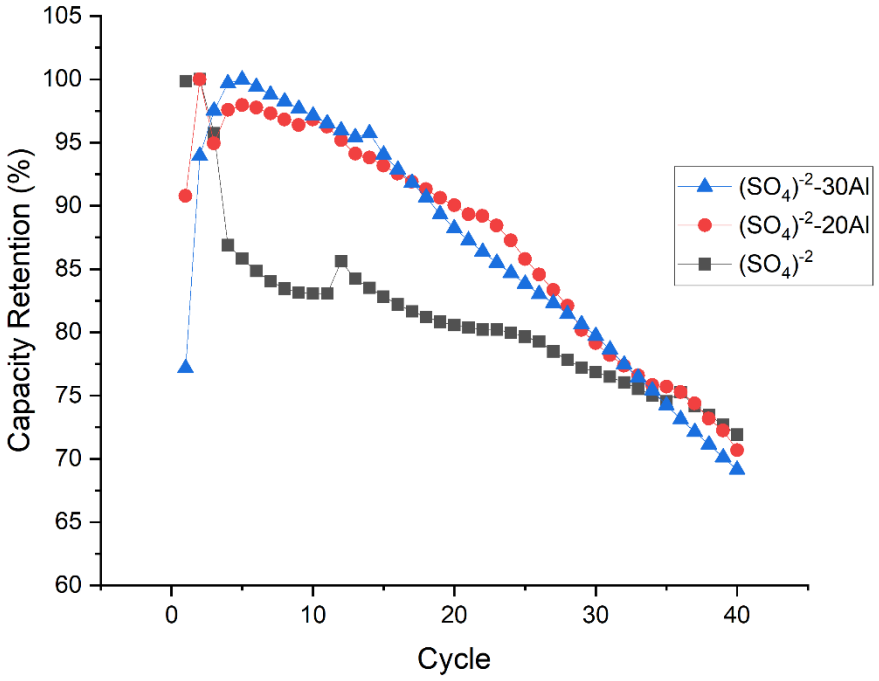


Figure 4-21. Effect of Al doping on the stability of $(SO_4)^{-2}$ based sample (100 mA/g for 3 cycles, rest of the cycles 400mA/g)

CHAPTER 5

CONCLUSION

Effects of precursor, dopant type, and dopant amount were investigated in this study. The findings can be summarized as follow:

1. Effects of $(NO_3)^{-1}$ on the performance of α-$Ni(OH)_2$
   The samples synthesized from $(NO_3)^{-1}$ have a low oxygen evolution rate and low mechanical stress. Thus, they have good stability and moderate capacity. It is the best option for self-discharge.
2. Effects of $(SO_4)^{-2}$ on the performance of α-$Ni(OH)_2$
   The samples show poor stability and tap density than others. It causes more mechanical stress.
3. Effects of Cl^{-1} on the performance of α-$Ni(OH)_2$
   It is a better option than $(NO_3)^{-1}$ for capacity and tap density but self-discharge performance is poor than $(NO_3)^{-1}$.
4. Effects of Co doping on the performance of α-$Ni(OH)_2$
   It increases stability, chargeability, and capacity in low doping levels.
5. Effects of Al doping on the performance of α-$Ni(OH)_2$
   It increases stability in high doping levels. It is non-toxic and cheap. But it causes chargeability and self-discharge problems. Not suitable to use with $(SO_4)^{-2}$.
6. Effects of Mn doping on the performance of α-$Ni(OH)_2$
   It acts as a beta stabilizer and requires a protective atmosphere. It increases chargeability and the best option for self-discharge

In summary, there is no best dopant or precursor for synthesizing. One should choose or combine dopants according to requirements. Especially, a low level of Co and a high level of Al can be used together to improve the performance of α-$Ni(OH)_2$.

REFERENCES

1) Li, J., Wei, M., Chu, W., & Wang, N. (2017). High-stable α-phase Nico double hydroxide microspheres via microwave synthesis for Supercapacitor Electrode Materials. Chemical Engineering Journal, 316, 277–287. https://doi.org/10.1016/j.cej.2017.01.057
2) Young, K.-H., Wang, L., Yan, S., Liao, X., Meng, T., Shen, H., & Mays, W. (2017). Fabrications of high-capacity alpha-ni(oh)2. *Batteries*, *3*(4), 6. https://doi.org/10.3390/batteries3010006
3) Zhao, T., Zhu, Y., Li, W., & Jian, X. (2017). Differences in the effects of aluminum/ytterbium/cobalt on the structural stability and electrochemical properties of nickel hydroxide. Materials Research Bulletin, 86, 257–267. https://doi.org/10.1016/j.materresbull.2016.10.029
4) Gamboa, S. (2001). Temperature, cycling, discharge current and self-discharge electrochemical studies to evaluate the performance of a pellet metal-hydride electrode. International Journal of Hydrogen Energy, 26(12), 1315–1318. https://doi.org/10.1016/s0360-3199(01)00066-0
5) Bode, H., Dehmelt, K., & Witte, J. (1966). Zur Kenntnis der nickelhydroxidelektrode—i.über das nickel (ii)-hydroxidhydrat. Electrochimica Acta, 11(8), 1079–1087. https://doi.org/10.1016/0013-4686(66)80045-2
6) Tsais, P.-J., & Chan, L. I. (2013). Nickel-based batteries: Materials and chemistry. Electricity Transmission, Distribution and Storage Systems, 315–316. https://doi.org/10.1533/9780857097378.3.309
7) Hall DS, Lockwood DJ, Bock C, MacDougall BR. 2015 Nickel hydroxides and related materials: a review of their structures, synthesis and properties. Proc. R. Soc. A 471: 20140792. http://dx.doi.org/10.1098/rspa.2014.0792
8) Wang, X., Li, Z., Zhang, J., Yan, H., Wang, C., Wu, F., Tian, A., Hong, X., Dong, W., & Yang, S. (2020). Effect of average interlayer spacing on

capacitance of NIMN layered double hydroxide. Chemical Engineering Journal, 398, 125618. https://doi.org/10.1016/j.cej.2020.125618

9) O'Grady, W. E., Pandya, K. I., Swider, K. E., & Corrigan, D. A. (1996). In situ x ray absorption near edge structure evidence for quadrivalent nickel in nickel battery electrodes. Journal of The Electrochemical Society, 143(5), 1613–1617. https://doi.org/10.1149/1.1836687
10) Desilvestro, J., Corrigan, D. A., & Weaver, M. J. (1988). Characterization of redox states of nickel hydroxide film electrodes by in situ surface Raman spectroscopy. Journal of The Electrochemical Society, 135(4), 885–892. https://doi.org/10.1149/1.2095818
11) Wang, C. Y., Zhong, S., Konstantinov, K., Walter, G., & Liu, H. K. (2002). Structural study of al-substituted nickel hydroxide. Solid State Ionics, 148(3-4), 503–508. https://doi.org/10.1016/s0167-2738(02)00095-4
12) Zou, X., Hao, J., Zhou, Y., Chen, F., Hu, Q., Xiang, B., Yang, H., & Deng, M. (2021). Electrochemical activation fabrication towards high-capacity nickel hydroxide electrode. Journal of Alloys and Compounds, 855, 157332. https://doi.org/10.1016/j.jallcom.2020.157332
13) Hu, M., Yang, Z., Lei, L., & Sun, Y. (2011). Structural transformation and its effects on the electrochemical performances of a layered double hydroxide. Journal of Power Sources, 196(3), 1569–1577. https://doi.org/10.1016/j.jpowsour.2010.08.041
14) Chen, W., Yang, Y., & Shao, H. (2011). Cation-exchange induced high power electrochemical properties of core–shell ni(oh)2@coooh. Journal of Power Sources, 196(1), 488–494. https://doi.org/10.1016/j.jpowsour.2010.07.026
15) Tsais, P.-J., & Chan, L. I. (2013). Nickel-based batteries: Materials and chemistry. Electricity Transmission, Distribution and Storage Systems, 315–316. https://doi.org/10.1533/9780857097378.3.309
16) Shangguan, E., Li, J., Guo, D., Guo, L., Nie, M., Chang, Z., Yuan, X.-Z., & Wang, H. (2015). A comparative study of structural and

electrochemical properties of high-density aluminum substituted α-nickel hydroxide containing different interlayer anions. Journal of Power Sources, 282, 158–168. https://doi.org/10.1016/j.jpowsour.2015.02.059

17) Ortiz, M., Becker, D., Garaventta, G., Visintin, A., Castro, E. B., & Real, S. G. (2011). Dynamic monitoring of structural changes in nickel hydroxide electrodes during discharge in batteries. Electrochimica Acta, 56(23), 7946–7954. https://doi.org/10.1016/j.electacta.2011.01.045
18) Li, J., Shangguan, E., Guo, D., Tian, M., Wang, Y., Li, Q., Chang, Z., Yuan, X.-Z., & Wang, H. (2014). Synthesis, characterization and electrochemical performance of high-density aluminum substituted α-nickel hydroxide cathode material for nickel-based rechargeable batteries. Journal of Power Sources, 270, 121–130. https://doi.org/10.1016/j.jpowsour.2014.07.098
19) Gilliam, R., Graydon, J., Kirk, D., & Thorpe, S. (2007). A review of specific conductivities of potassium hydroxide solutions for various concentrations and temperatures. International Journal of Hydrogen Energy, 32(3), 359–364. https://doi.org/10.1016/j.ijhydene.2006.10.062
20) Ayeb, A., & Notten, P. H. L. (2008). The oxygen evolution kinetics in sealed rechargeable nimh batteries. Electrochimica Acta, 53(19), 5836–5847. https://doi.org/10.1016/j.electacta.2008.03.023
21) Shangguan, E., Zhang, H., Wu, C., Cai, X., Wang, Z., Wang, M., Li, L., Wang, G., Li, Q., & Li, J. (2020). Coal-layered double hydroxide nanosheets-coated spherical nickel hydroxide cathode materials with enhanced high-rate and cycling performance for alkaline nickel-based secondary batteries. Electrochimica Acta, 330, 135198. https://doi.org/10.1016/j.electacta.2019.135198
22) Ikoma, M., Hoshina, Y., Matsumoto, I., & Iwakura, C. (1996). Self-discharge mechanism of sealed-type nickel/metal-hydride battery. Journal of The Electrochemical Society, 143(6), 1904–1907. https://doi.org/10.1149/1.1836922

23) Shukla, A. K., Venugopalan, S., & Hariprakash, B. (2009). Secondary batteries – nickel systems | nickel–cadmium: Overview. Encyclopedia of Electrochemical Power Sources, 452–458. https://doi.org/10.1016/b978-044452745-5.00153-2

24) Zhang, Z. J., Zhu, Y. J., Bao, J., Lin, X. R., & Zheng, H. Z. (2011). Electrochemical performance of multi-element doped α-nickel hydroxide prepared by supersonic co-precipitation method. Journal of Alloys and Compounds, 509(25), 7034–7037. https://doi.org/10.1016/j.jallcom.2011.03.104

25) Oliva, P., Leonardi, J., Laurent, J. F., Delmas, C., Braconnier, J. J., Figlarz, M., Fievet, F., & Guibert, A. (1982). Review of the structure and the electrochemistry of nickel hydroxides and oxy-hydroxides. Journal of Power Sources, 8(2), 229–255. https://doi.org/10.1016/0378-7753(82)80057-8

26) Wang, X., Sebastian, P. J., Millan, A. C., & Parkhutik, P. V. (2015). Electrochemical study of nanostructured multiphase nickel hydroxide. Journal of New Materials for Electrochemical Systems.

27) Dixit, M., Kamath, P. V., & Gopalakrishnan, J. (1999). Zinc-substituted α-nickel hydroxide as an electrode material for alkaline secondary cells. Journal of The Electrochemical Society, 146(1), 79–82. https://doi.org/10.1149/1.1391567

28) Melhem, Z., Chan, S. L., & TSAI, P. J. (2013). Nickel-based batteries: materials and chemistry. In Electricity transmission, distribution and Storage Systems (pp. 309–310). essay, Woodhead Publishing.

29) Ash, B., Nalajala, V. S., Popuri, A. K., Subbaiah, T., & Minakshi, M. (2020). Perspectives on nickel hydroxide electrodes suitable for rechargeable batteries: Electrolytic vs. chemical synthesis routes. Nanomaterials, 10(9), 1878. https://doi.org/10.3390/nano10091878

30) Guerlou-Demourgues, L., & Delmas, C. (1994). Crystal Chemistry and electrochemical behavior of new Manganese substituted nickel hydroxides. MRS Proceedings, 369. https://doi.org/10.1557/proc-369-81

31) Kamath, P. V., Dixit, M., Indira, L., Shukla, A. K., Kumar, V. G., & Munichandraiah, N. (1994). Stabilized α-ni (OH) 2 as electrode material for alkaline secondary cells. Journal of The Electrochemical Society, 141(11), 2956–2959. https://doi.org/10.1149/1.2059264

32) Zhang, Z.-ju, Zhu, Y.-juan, Bao, J., Zhou, Z.-jun, Ye, X.-cong, & XU, Q.-sheng. (2011). Effect of ultrasonic on structure and electrochemical performance of α-ni(oh)2 electrodes. Transactions of Nonferrous Metals Society of China, 21(12), 2654–2659. https://doi.org/10.1016/s1003-6326(11)61106-0

33) Shangguan, E., Chang, Z., Tang, H., Yuan, X.-Z., & Wang, H. (2011). Comparative structural and electrochemical study of high density spherical and non-spherical Ni(OH)2 as cathode materials for ni–metal hydride batteries. Journal of Power Sources, 196(18), 7797–7805. https://doi.org/10.1016/j.jpowsour.2011.05.013

34) Huang, J., Cao, D., Lei, T., Yang, S., Zhou, X., Xu, P., & Wang, G. (2013). Structural and electrochemical performance of al-substituted β-ni(oh)2 nanosheets electrodes for nickel metal hydride battery. Electrochimica Acta, 111, 713–719. https://doi.org/10.1016/j.electacta.2013.08.1

35) Yang, L. J., Gao, X. P., Wu, Q. D., Zhu, H. Y., & Pan, G. L. (2007). Phase distribution and electrochemical properties of al-substituted nickel hydroxides. The Journal of Physical Chemistry C, 111(12), 4614–4619. https://doi.org/10.1021/jp0655468

36) Aghazadeh, M., Ghaemi, M., Sabour, B., & Dalvand, S. (2014). Electrochemical preparation of α-ni(oh)2 ultrafine nanoparticles for high-performance supercapacitors. Journal of Solid State Electrochemistry, 18(6), 1569–1584. https://doi.org/10.1007/s10008-014-2381-7

37) Li, X., Xia, T., Li, Z., Dong, H., & Li, S. (2011). MN-substituted nickel hydroxide prepared by ball milling and its electrochemical properties. Journal of Alloys and Compounds, 509(32), 8246–8250. https://doi.org/10.1016/j.jallcom.2011.05.096

38) Guerlou-Demourgues, L., & Delmas, C. (1994). New Manganese-substituted nickel hydroxides. Journal of Power Sources, 52(2), 275–281. https://doi.org/10.1016/0378-7753(94)02024-8

39) Jian, X. W., Zhu, Y. J., Li, W. H., & Zhao, T. Q. (2016). Crystal phase, structure stability and electrochemical performance of Co/Cu/Al-substituted nano-sized alpha nickel hydroxide. Applied Physics A, 122(10). doi:10.1007/s00339-016-0443-7

40) Liu, C., Chen, S., & Li, Y. (2011). Synthesis and electrochemical performance of α-nickel hydroxide codoped with Al3 and Ca2. Ionics, 18(1-2), 197-202. doi:10.1007/s11581-011-0593-8

41) Hu, M., Ji, X., Lei, L., & Lu, X. (2013). The effect of cobalt on the electrochemical performances of ni–al layered double hydroxides used in ni–M(H) battery. Journal of Alloys and Compounds, 578, 17–25. https://doi.org/10.1016/j.jallcom.2013.04.156

42) Xu, Q., Zhu, Y., Han, Q., Zhao, R., Zhuang, Y., Liu, Y., Zhang, S., & Miao, C. (2014). Preparation of YB-substituted α-ni(oh)2 and its physicochemical properties. Journal of Alloys and Compounds, 584, 1–6. https://doi.org/10.1016/j.jallcom.2013.08.097

43) W.-K. Hu, D. Noréus, Alpha nickel hydroxides as lightweight nickel electrode materials for alkaline rechargeable cells, Chem. Mater. 15 (2003) 974-978.

44) H. Chen, J.M. Wang, T. Pan, Y.L. Zhao, J.Q. Zhang, C.N. Cao, The structure and electrochemical performance of spherical Al-substituted α-Ni(OH)2 for alkaline rechargeable batteries, J. Power Sources 143 (2005) 243-255.

45) Liu, K., Zhou, W., Zhu, D., He, J., Li, J., Tang, Z., Huang, L., He, B., & Chen, Y. (2018). Excellent high-rate capability of micron-sized co-free α-ni(oh)2 for high-power Ni-MH Battery. Journal of Alloys and Compounds, 768, 269–276. https://doi.org/10.1016/j.jallcom.2018.07.158